

# Charge order and loop currents in hole-doped cuprates

Yuxuan Wang, Andrey Chubukov

*Department of Physics, University of Wisconsin, Madison, WI 53706, USA*

We analyze charge order in hole-doped cuprates. We show that magnetically-mediated interaction, which is known to give rise to non-Fermi liquid behavior in the normal state and  $d$ -wave superconductivity, also gives rise to charge order with momenta  $Q_x = (2Q, 0)$  and  $Q_y = (0, 2Q)$ , as seen in the experiments. We show that the emerging charge order is of stripe type (it appears with  $Q_x$  or  $Q_y$ , but not with both). We further show that a stripe charge order parameter has two components: one is incommensurate density variation, another is incommensurate current. Such an order breaks time reversal symmetry and generates loop currents. We show that loop current order sets up at a higher  $T^* > T_{\text{CDW}}$ , when the density and the current components form a composite order with zero total momentum. We further show that  $T_{\text{CDW}}(x)$  and  $T^*(x)$  terminate at  $T = 0$  at some finite doping  $x$  and set up the second quantum critical point at some distance away from the magnetic one. We argue that our theory provides the “missing link” in the spin-fluctuation scenario for the cuprates.

## I. INTRODUCTION

Intensive experimental studies of hole-doped cuprates over the last few years have provided strong indications that much discussed pseudogap region is a state (or even a set of states) with broken symmetry<sup>1</sup>. First, polarized elastic neutron scattering measurements detected the emergence of an intra-unit cell magnetic order<sup>2,3</sup> below a certain  $T^*(x)$ , and measurements of the Kerr angle at optical frequencies detected<sup>4</sup> a polar Kerr effect below about the same temperature. The most natural (although not the only possible<sup>5</sup>) interpretation of these two measurements is that  $T^*$  is associated with the onset of time-reversal symmetry breaking. Second, X-ray and neutron scattering data on  $\text{La}_{1.875}\text{Ba}_{0.125}\text{CuO}_4$  strongly indicate<sup>6,7</sup> that lattice rotational symmetry is broken from  $C_4$  down to  $C_2$ . Evidence for rotational symmetry breaking has been also found in neutron scattering data on YBCO<sup>8</sup> and in STM data on  $\text{Bi}_2\text{Sr}_2\text{CaCu}_2\text{O}_{8+\delta}$ , at energies comparable to  $T^*$  (Ref. [9]). Third, recent NMR and sound velocity measurements in a magnetic field  $H$  (Refs. [10–13]) found a charge density-wave (CDW) order at  $H \geq 20T$ . A static short-range incommensurate CDW order with momenta  $Q_x = (2Q, 0)$  and/or  $Q_y = (0, 2Q)$  has been also found in X-ray measurements on YBCO (Refs.[14,15]),  $\text{Bi}_2\text{Sr}_{2-x}\text{La}_x\text{CuO}_{6+\delta}$  (Ref. [16]), and  $\text{Bi}_2\text{Sr}_2\text{CaCu}_2\text{O}_{8+\delta}$  (Ref. [17]), and  $2Q$  was determined to be equal to the distance between neighboring hot spots –points where the Fermi surface (FS) intersects with magnetic Brillouin zone boundary<sup>16,17</sup>.

Quantum oscillation measurements<sup>18</sup> and measurements of Hall and Seebeck coefficients<sup>19</sup> were also interpreted as evidence of the feedback effect from the CDW order on fermions. The onset temperature  $T_{\text{CDW}}(x)$  of the CDW order (more accurately, of strong charge fluctuations) was found to systematically lie below  $T^*(x)$ . Fourth, ARPES measurements deep under the superconducting dome have found<sup>20</sup> a change of system behavior at a certain doping, and were interpreted as evidence for the existence of a quantum-critical point (QCP) at

$x = x_{cr}$ , at which a new order emerges and competes with superconductivity (SC). The extrapolations from  $T > T_c$  to  $T = 0$  seem to indicate that  $T^*(x)$  and  $T_{\text{CDW}}(x)$  lines tend to the same value at  $T = 0$ . It is then natural to associate this QCP with the simultaneous breaking of the translational symmetry, associated with  $T_{\text{CDW}}$ , and the one associated with  $T^*$ , for which the most natural candidate is time-reversal symmetry.

These and related experimental data<sup>21?</sup> pose a challenge to the theory. System behavior outside the pseudogap region can be reasonably well described within a theoretical framework that fermions interact by exchanging quanta of collective excitations. The most natural interaction of this kind is the exchange of spin fluctuations, peaked at or near antiferromagnetic momenta  $(\pi, \pi)$ . The corresponding spin-fluctuation approach<sup>23–26</sup> yields a  $d$ -wave superconductivity and non-Fermi liquid behavior of fermionic self-energy and optical conductivity<sup>27</sup>. At the same time, until recently, this approach was believed to be incapable to describe symmetry breaking in the pseudogap phase. Other possible explanations of a pseudogap have been proposed, like loop-current order<sup>28</sup>,  $d$ -wave current order<sup>29,30</sup>, precursor to Mott physics<sup>31–35</sup>, or precursors to either magnetism<sup>36–38</sup> or superconductivity<sup>39,40</sup>.

The spin-fluctuation scenario was revitalized by Metlitski and Sachdev<sup>41</sup> who found that the spin-mediated interaction is attractive not only in the  $d$ -wave superconducting channel but also in the  $d$ -wave CDW channel, at momenta  $2k_{hs}$ , where  $k_{hs}$  is the momentum of one of hot spot on a Fermi surface (FS). In real space, a  $d$ -wave CDW instability implies a bond order. The analysis of  $2k_{hs}$  CDW instability within spin-fluctuation approach was extended by Efetov, Meier, and Pépin<sup>42</sup>, who argued that the pseudogap behavior may be the consequence of the competition between bond order and superconductivity. This scenario is appealing from theory perspective and allows one to explain some experimental data<sup>13,43</sup>. However, it has three discrepancies with the experiments: (i) the momentum  $2k_{hs}$  is directed along Brillouin zone diagonal, while CDW momentum detected by resonant

X-ray scattering is along horizontal or vertical axis (with  $Q_x = (Q, 0)$  or  $Q_y = (0, Q)$ , respectively, Refs.[16,17]), (ii) bond-order instability is always secondary to the SC instability, while experiments see the development of charge order above superconducting  $T_c$ , (iii) the bond order with  $Q = 2k_{hs}$  does not explain Kerr and elastic neutron scattering measurements<sup>2,4</sup> which point to the existence of an order with zero momentum below  $T^* > T_{CDW}$ .

In this paper we present a different scenario for the pseudogap due to spin-fluctuation exchange. We argue that magnetically-mediated interaction is also attractive in CDW channel with  $Q_x$  and  $Q_y$ , and the attraction is strong enough to give rise to a CDW instability with these momenta. The order has both on-site and bond components. We show that the CDW order  $\Delta_k^Q = \langle c_{k+Q}^\dagger c_{k-Q} \rangle$  is of stripe type – it appears with only  $Q_x$  or  $Q_y$ , but not with both, and breaks lattice rotational symmetry (an alternative would be a checkerboard order, with equal participation of  $Q_x$  and  $Q_y$  components). We next take a more careful look at the dependence of  $\Delta_k^Q = \langle c_{k+Q}^\dagger c_{k-Q} \rangle$  with, say,  $Q_y$ , on the center of mass momentum  $k$ . We argue that  $\Delta_k^Q$  generally has two components –one is even in  $k$ , the other is odd (e.g.,  $\cos k$  and  $\sin k$ , respectively). Both components are present because  $k$  is not a symmetry point in the Brillouin zone (for charge order with diagonal  $\mathbf{Q} = 2\mathbf{k}_{hs}$ , only even in  $k$  solution is possible because then center of mass momentum is located at  $k = 0$ ). If we approximate  $\Delta_k^Q$  by its value for  $\mathbf{k} \pm \mathbf{Q}$  right at hot spots, we find that  $T_{CDW}$  for both components is the same. In the full lattice calculation, the onset temperature for even component is larger, in agreement with Ref. [44], but the one for the odd component remains close. We derive Ginzburg-Landau functional for coupled even and odd components of  $\Delta_k^Q$  and show that they appear with a relative phase factor  $\pm\pi/2$ , the corresponding  $\Delta_k^Q$  is then necessarily a complex vector, with both even and odd components present. Because  $\Delta_k^Q$  transforms into  $(\Delta_{-k}^Q)^* \equiv \Delta_{-k}^Q$  under time reversal, a complex CDW order parameter breaks time-reversal symmetry. We show that an even component of  $\Delta_k^Q$  represents variation of a density  $\delta\rho(r) \propto \cos 2Qr_y$  and an odd component represents a fermionic current  $j_x(r) \propto \sin 2Qr_y$  (for our choice of  $Q = Q_y$ ). We argue that a simultaneous presence of  $\delta\rho(r)$  and  $j_x(r)$ , oscillating with the phase difference  $\pm\pi/2$ , gives rise to loop currents, which generate an orbital magnetic field  $H_z$ .

We next show, using the same strategy as in the analysis of the nematic order in Fe-pnictides<sup>46</sup>, that, before charge order sets in at  $T_{CDW}$ , the systems undergoes a preemptive instability at  $T^* > T_{CDW}$ , at which the density and the current components of  $\Delta_k^Q$  form a composite order with zero total momentum. In between  $T^*$  and  $T_{CDW}$ ,  $\langle \delta\rho(r) \rangle = \langle j_x(r) \rangle = 0$ , but  $\Upsilon \propto \langle \delta\rho(r)j_x(r) \rangle$  becomes non-zero. Under time reversal,  $\Upsilon$  transforms into  $-\Upsilon$ , hence this order breaks time reversal symme-

try. We will show that it gives rise to loop currents, like CDW order does, however loop current order with  $q = 0$  emerges at a higher temperature than CDW order itself. We identify  $T^*$  with the onset of Kerr effect and elastic  $q = 0$  neutron signal, and identify  $T_{CDW}$  with the onset of charge order seen in X-ray and other measurements. Our scenario is different from a recent proposal<sup>47</sup> of two transitions at  $T^*$  and  $T_{CDW}$  – in their case CDW order emerges with a different momentum, due to strong SC fluctuations.

We also consider doping evolution of  $T^*$  and  $T_{CDW}$  and the interplay between charge order and superconductivity. We argue that near a magnetic QCP, when spin-fluctuations are near-critical,  $T_{CDW} \leq T_c$ , however  $T^*$  is larger than  $T_{CDW}$  and well may be higher than  $T_c$  (Fig. 3 (a), (b)). We show that  $T_{CDW}$  and  $T^*$  decrease when magnetic correlation length  $\xi$  decreases and vanish at some finite  $\xi$ , setting up a charge QCP at some distance from the magnetic instability (see Fig. 3(b)). We combine  $T_c$ ,  $T_{CDW}$ , and  $T^*$  lines into the phase diagram, which we show in Fig. 3(c). We argue that the reduction of  $T_c$  in the underdoped regime is likely not a fluctuation effect associated with enhanced symmetry, as Ref. [42] suggested, but rather just the result of a competition between SC and loop-current order, both produced by the same underlying spin-fluctuation exchange interaction, much like  $T_c$  decreases in underdoped pnictides due to competition with SDW order in a model in which SC and SDW originate from the same 4-fermion pair-hopping interaction<sup>48,49</sup>. We compare our theoretical phase diagram with the one for hole-doped cuprates and present quantitative comparison of our theory with ARPES data, including Fermi arcs in the normal state and the doping evolution of the spectral function at low  $T$ , when the systems moves from a pure SC state into a state where SC and charge order co-exist.

## II. THE MODEL AND THE THEORETICAL FRAMEWORK

We use the same spin-fermion model as in earlier studies of magnetically-mediated  $d$ -wave superconductivity<sup>23,25</sup> and non-Fermi liquid physics<sup>26,41</sup> outside of pseudogap region. The model describes low-energy fermions with the FS shown in Fig. 1 and with 4-fermion interaction mediated by soft collective excitations in the spin channel, peaked at or near  $(\pi, \pi)$ . We focus on hot regions on the FS, for which shifting  $\mathbf{k}_F$  by  $\mathbf{k}_F + (\pi, \pi)$  keeps a fermion near the FS, and expand fermionic dispersion near a hot spot as  $\epsilon_k = v_{F,\mathbf{k}}(k_\perp + \kappa k_\parallel^2/k_F)$ , where  $v_{F,\mathbf{k}}$  is a Fermi velocity at a hot spot,  $k_\parallel$  is a deviation from a hot spot along the FS, and dimensionless  $\kappa$  specifies the curvature of the FS. The Fermi velocities at hot spots  $\mathbf{k}_1$ ,  $\mathbf{k}_2$  and  $\mathbf{k}_3 = \mathbf{k}_1 + (\pi, \pi)$ ,  $\mathbf{k}_4 = \mathbf{k}_2 + (\pi, \pi)$  in Fig. 1 are  $\mathbf{v}_{F,\mathbf{k}_1} = (v_x, v_y)$ ,  $\mathbf{v}_{F,\mathbf{k}_2} = (v_x, -v_y)$ ,  $\mathbf{v}_{F,\mathbf{k}_3} = (-v_y, -v_x)$ , and  $\mathbf{v}_{F,\mathbf{k}_4} = (-v_y, v_x)$ . The am-

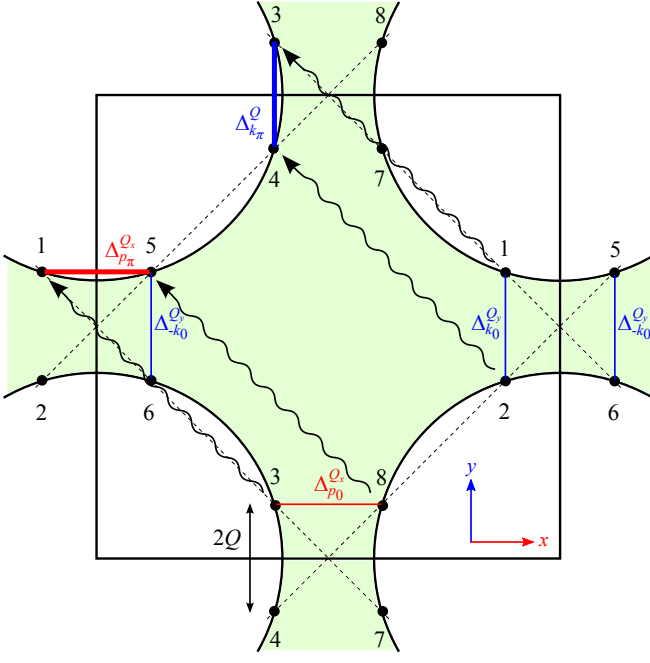


FIG. 1: The Fermi surface, Brillouin zone and magnetic Brillouin zone (dashed line). Hot spots are defined as intersections of the FS with magnetic Brillouin zone. The hot spot pairs 1-2 and 3-4 denotes the CDW pairing we consider. They are coupled through the antiferromagnetic exchange interaction peaked at momentum  $(\pi, \pi)$ , as shown by the dashed arrows.

plitude of the Fermi velocity  $v_{F,\mathbf{k}} = \sqrt{v_x^2 + v_y^2}$  and the value of  $\kappa$  are the same at all hot spots. The effective 4-fermion interaction mediated by soft spin excitations is  $\bar{g}\chi(q)c_{k+q,\alpha}^\dagger\sigma_{\alpha\beta}c_{k,\beta}c_{p-q,\gamma}^\dagger\sigma_{\gamma\delta}c_{p,\delta}$ , where  $k = (\mathbf{k}, \omega_m)$ ,  $q = (\mathbf{q}, \Omega_m)$ ,  $\omega_m(\Omega_m)$  are fermionic (bosonic) Matsubara frequencies, and  $\chi(q) = \chi(\mathbf{q}, \Omega_m) = 1/(\mathbf{q}^2 + \xi^{-2} + \gamma|\Omega_m|)$ , where the last term is the Landau damping with the coefficient  $\gamma = 4\bar{g}/(\pi|v_y^2 - v_x^2|)$  (Ref. [26]). It contains the same  $\bar{g}$  as the overall factor in spin-mediated interaction because Landau damping of collective spin excitations originates from the same spin-fermion interaction.

Following earlier works<sup>26,41,42</sup>, we assume that the coupling  $\bar{g}$  is small compared to the Fermi energy  $E_F = v_F k_F/2$  and focus on instabilities which occur at energies well below  $E_F$  and at  $\xi^{-1} \geq 0$ , before the system becomes magnetically ordered. One such instability is towards a  $d$ -wave superconductivity<sup>23-25,50</sup>. It involves fermions from cold and lukewarm regions on the FS (with the self-energy  $\Sigma(k_{\parallel}, \omega_m) \propto \sqrt{\omega_m}$  and  $\Sigma(k_{\parallel}, \omega_m) \propto \omega_m/|k_{\parallel}|$ , respectively), and, taken alone (i.e., without competition with CDW order) occurs at  $T_c = T_c(\xi)$ , which is nonzero at all  $\xi$  and interpolates between  $T_c(\xi) \approx 0.04\bar{g}$  at large  $\xi$ , with weak dependence on  $v_x/v_y$ , (Refs. [50,51]), and BCS-like result  $T_c(\xi) \sim (\bar{g}/\lambda^2)e^{-1/\lambda}$ , at smaller  $\xi \ll E_F/\bar{g}$ , when dimensionless coupling  $\lambda = 3\bar{g}/(4\pi v_F \xi^{-1})$  is small (see panel b in Fig. 3). Another instability, considered in<sup>41,42</sup>, is towards a  $d$ -wave charge bond or-

der with diagonal momentum  $2\mathbf{k}_{hs} = 2Q(1, \pm 1)$ , where  $\mathbf{k}_{hs} = (Q, \pi \pm Q)$ . This instability develops at  $T_{BO}(\xi)$ , which is smaller than  $T_c(\xi)$ , although rather close to it at  $\xi \rightarrow \infty$  (Refs. [41,42]). We analyzed the form of  $T_{BO}(\xi)$  and found (see Supplementary Material (SM)) that bond-order instability becomes a threshold problem at a finite  $\xi$ , and  $T_{BO}(\xi)$  vanishes at a certain  $\xi$ , when  $\lambda \log(E_F/(\bar{g}\kappa)) = O(1)$ , where, we remind,  $\kappa$  is the curvature of the FS.

We looked into another CDW channel, this time with momentum  $Q_x = (2Q, 0)$  or  $Q_y = (0, 2Q)$ . This pairing involves fermions from hot/lukewarm regions 1-2, 3-4, etc. in Fig. 1. The analysis of a potential CDW instability involving such fermions is a bit tricky, because fermions in the regions connected by the interaction peaked by  $(\pi, \pi)$  (e.g., regions 1-2 and 3-4 in Fig. 1) are different in the sense that the values of parallel (antiparallel) velocities are  $v_x$  ( $v_y$ ) in the first set and  $-v_y$  ( $-v_x$ ) in the second, and  $v_x$  and  $v_y$  are different at a hot spot. Accordingly, the CDW order parameter  $\Delta_k^Q = \langle c_{k+Q,\alpha}^\dagger c_{k-Q,\alpha} \rangle$  does not obey a particular symmetry relation under  $\mathbf{k} \rightarrow \mathbf{k} + (\pi, \pi)$ , and one has to solve the  $2 \times 2$  coupled set of equations for  $\Delta_k^Q$  and  $\Delta_{k+\pi}^Q$  (where  $k + \pi$  is a short-cut for  $\mathbf{k} + (\pi, \pi)$ ). The solution is (see SM)

$$\begin{aligned} \Delta_{k_0}^Q &= -S_1 \Delta_{k_\pi}^Q \log \frac{\bar{g}}{T}, \\ \Delta_{k_\pi}^Q &= -S_2 \Delta_{k_0}^Q \log \frac{\bar{g}}{T}, \end{aligned} \quad (1)$$

where  $S_1$  and  $S_2$  (both positive) depend on the ratio of  $v_x/v_y$  but not on  $\bar{g}$ , which cancels out between the overall factor in the spin-fermion interaction and in the Landau damping. This cancellation is typical for an instability mediated by a massless Landau-overdamped collective mode<sup>51</sup>.

In the limit when  $v_x = 0$  (i.e., when the velocities at hot spots 1 and 2 are nearly antiparallel, and the ones at hot spots 3 and 4 are nearly parallel), we have  $S_1 = 0.072$  and  $S_2 = 0.407$ . For a finite  $v_x/v_y$ , the values of  $S_1$  and  $S_2$  are closer to each other.

The negative overall sign in the r.h.s of (1) implies that there must be a sign change between  $\Delta_{k_0}^Q$  and  $\Delta_{k_\pi}^Q$ . A logarithmical dependence on  $T$  in turn implies that the CDW instability does emerge below a certain  $T_{CDW} = O(\bar{g})$ , which is of the same order as  $T_c(\xi \rightarrow \infty)$ . (From equation (1),  $T_{CDW} \sim \bar{g}e^{-1/(S_1 S_2)^{1/2}}$ ). Because  $\Delta_k^Q$  and  $\Delta_{k_\pi}^Q$  differ in magnitude, their contributions to charge density modulation in real space do not cancel, i.e., below the instability the system develops a true CDW order proportional to  $\Delta_{k_0}^Q + \Delta_{k_\pi}^Q$ , together with a bond order, proportional to  $\Delta_{k_0}^Q - \Delta_{k_\pi}^Q$ . The full solution for CDW instability with  $Q_x$  ( $Q_y$ ) is more involved as one has to keep the frequency dependencies of  $\Delta_{k_0}^Q$  and  $\Delta_{k_\pi}^Q$  and solve the set of two coupled integral equations for

frequency-dependent CDW vertices. We found (see SM) that the full solution still shows that the system develops a CDW instability below a certain  $T_{\text{CDW}}$  with either horizontal or vertical momentum  $Q_x$  or  $Q_y$ . We compare  $T_{\text{CDW}}$  and superconducting  $T_c$  below, when we discuss the phase diagram.

### A. The structure of charge order

We now consider the structure of  $\Delta_k^Q$ . We first address the issue whether CDW order develops simultaneously with both  $Q_x$  and  $Q_y$ , in which case it preserves the underlying lattice  $C_4$  symmetry and gives rise to checkerboard charge order in the real space, or with either  $Q_x$  or  $Q_y$ , in which case it spontaneously breaks  $C_4$  symmetry down to  $C_2$  and gives rise to stripe order. The order with  $Q_x$  corresponds to CDW between fermions in regions 1-2 and 3-4 in Fig. 1 and the order with  $Q_y$  corresponds to CDW between fermions in regions 1-5 and 3-8. To distinguish between the two cases, we introduce two bosonic fields  $\Delta_x = \Delta_k^Q$  with  $Q = Q_x$  and similarly  $\Delta_y$ , apply Hubbard-Stratonovich transformation to the fermionic action, integrate over fermions, and obtain the effective action  $\mathcal{S}_{\text{eff}}(\Delta_x, \Delta_y)$  for the two CDW order parameters. The action has a conventional form

$$\mathcal{S}_{\text{eff}}(\Delta_x, \Delta_y) = \alpha (\Delta_x^2 + \Delta_y^2) + \beta_1 (\Delta_x^4 + \Delta_y^4) + 2\beta_2 \Delta_x^2 \Delta_y^2 \quad (2)$$

We found  $\alpha = a(T - T_{\text{CDW}})$ ,  $a > 0$ , and  $\beta_1 > 0$ , as is required for the transition to be second-order. One can easily make sure that the system develops a checkerboard order if  $\beta_1 > |\beta_2|$  and stripe order if  $|\beta_2| > \beta_1$ . The two coefficients,  $\beta_1$  and  $\beta_2$ , are expressed via the square diagrams with four fermionic propagators. We evaluated the diagrams (see SM) and found that  $\beta_2$  well exceeds  $\beta_1$ :  $\beta_2/\beta_1 \sim E_F/T \gg 1$ . As a result, the effective action (2) unambiguously yields a stripe CDW order. Phenomenological arguments for stripe charge order in hole-underdoped cuprates have been displayed earlier<sup>52</sup>, and our microscopic analysis is consistent with earlier works. We caution, however, that more accurate treatment is needed when CDW order emerges either from a pre-existing superconducting state, or in the presence of strong superconducting fluctuations.

We next consider in more details the form of the solution for, say,  $Q_y = (0, 2Q)$ . By construction, the order parameter satisfies  $(\Delta_k^Q)^* = \Delta_{-k}^{-Q}$ . This implies that incommensurate charge order parameter has an overall phase factor associated with the breaking of  $U(1)$  symmetry. However, this condition does not specify how  $\Delta_k^Q$  changes under  $k \rightarrow -k$ . For set 1-2 and 3-4 in Fig. 1 relevant  $k$  are near  $k_0 = (\pi - Q, 0)$  and  $k_\pi = (-Q, \pi)$ . Another set of coupled equations for  $\Delta_k^Q$  and  $\Delta_{k+\pi}^Q$  can be obtained by choosing  $k$  near  $\bar{k}_0 = -k_0 \equiv (\pi + Q, 0)$  and  $\bar{k}_\pi = -k_\pi$  (the set 5-6 and 7-8 in Fig. 1). As long as typical  $|k - k_0|$  are smaller than  $2Q$  (i.e., as long as  $T_{\text{CDW}}$

is smaller than, roughly,  $E_F|Q/\pi|$ ), the two regions are disconnected and can be considered independent on each other. In this situation, the gap equation allows for two types of solutions for  $\Delta_k^Q$ : the one which is even under  $k \rightarrow -k$  ( $\Delta_1^Q$ ) and the one which is odd ( $\Delta_2^Q \text{sgn}(k)$ ). We emphasize that the possibility to have two types of solutions is specific to CDW order with  $Q_y$  ( $Q_x$ ). For a charge order with a diagonal  $Q$ , the center of mass momentum is at  $k = 0$ , and only even in  $k$  solution is possible. One can easily check<sup>44</sup> that under time reversal  $\Delta_k^Q \rightarrow \Delta_{-k}^Q$ , hence the odd in  $k$  solution for  $\Delta_k^Q$  changes sign under time-reversal.

To see whether the system prefers to develop both even and odd in  $k$  solutions below  $T_{\text{CDW}}$  or only one of them, we again analyzed the effective action, this time in terms of  $\Delta_1^Q$  and  $\Delta_2^Q$ . Applying again Hubbard-Stratonovich transformation and integrating over fermions near the hot spots, we obtain

$$\begin{aligned} \mathcal{S}_{\text{eff}}(\Delta_1^Q, \Delta_2^Q) = & \alpha \left( |\Delta_1^Q|^2 + |\Delta_2^Q|^2 \right) + \beta_1 \left( |\Delta_1^Q|^4 + |\Delta_2^Q|^4 \right) \\ & + 2\beta_1 \left( \Delta_1^Q (\Delta_2^Q)^* + (\Delta_1^Q)^* \Delta_2^Q \right)^2 + \dots \end{aligned} \quad (3)$$

where  $\beta_1 > 0$  is the same as in (2) and dots stand for higher-order terms. An analysis of this equation shows that the relative phase between  $\Delta_1^Q$  and  $\Delta_2^Q$  is  $\pm\pi/2$ . Without loss of generality we can set  $\Delta_1^Q$  to be real, in which case  $\Delta_2^Q$  is imaginary. The constraint  $(\Delta_k^Q)^* = \Delta_{-k}^{-Q}$  then requires  $\Delta_1^Q$  and  $\Delta_2^Q$  to be an even and an odd function of  $Q$ , respectively. The full solution for  $\Delta_k^Q$  is then

$$\Delta_k^Q = \Delta_1^Q \pm i|\Delta_2^Q| \text{sgn}(k) \text{sgn}(Q). \quad (4)$$

This  $\Delta_k^Q$  does not break parity, but it breaks time reversal symmetry because under time reversal  $\Delta_k^Q$  transforms into  $(\Delta_{-k}^{-Q})^* = \Delta_{-k}^Q$ . The choice of relative sign in (4) specifies one of two non-equivalent solutions which transform into each other under time-inversion. The order parameter (4) is similar, but not equivalent, to incommensurate complex  $d$ -density wave order proposed in [53,54].

In real space, the two components of  $\Delta_k^Q$  in (4) represent incommensurate modulation of fermionic density  $\delta\rho(r) \propto \Delta_1^Q \cos 2Qr_y$  and incommensurate bond current  $j_x(r) \propto |\Delta_2^Q| \sin 2Qr_y \sin Q$ . The current runs into  $x$  direction and oscillates in sign as a function of  $r_y$  (see Fig. 2). The density modulation creates excess or reduction of charge also along  $y$  direction, in anti-phase with the current. The current lines have to close at the boundary, and it is natural to expect that they close through the regions of excess charge, as shown in Fig 2. This creates a set of loop currents with circulation along the same direction, which in turn generate a uniform orbital magnetic field  $H_z$  at distances larger than  $\pi/(2Q)$ . The structure of loop currents and a magnetic field at distances smaller

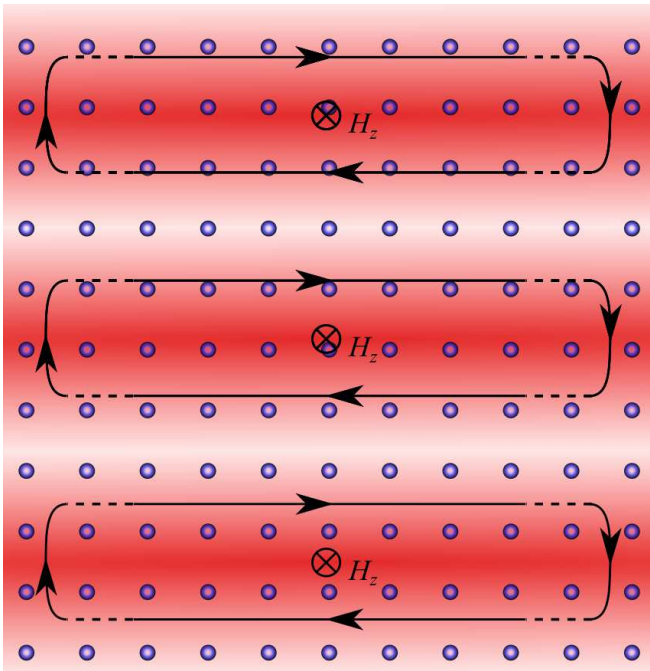


FIG. 2: Loop currents at distances larger than  $\pi/(2Q)$  as the result of CDW order which contains charge density modulation and bond current order. Both are oscillating as a function of  $r_y$  with  $\pm\pi/2$  phase difference, i.e., the charge density is maximized at  $r_y$  when the current vanishes and vice versa. The structure of the currents at distances smaller than  $\pi/(2Q)$  is beyond the scope of the present paper.

than  $\pi/(2Q)$ ) can be more involved, and the analysis of it is beyond the scope of the present paper. (Examples of more complex microscopic realizations of  $q = 0$  order are presented in [28].)

### B. Preemptive loop-current order

In the mean-field treatment of the Ginzburg-Landau functional of equation (3), both density and current components of  $\Delta_k^Q$  (i.e.,  $\Delta_1^Q$  and  $\Delta_2^Q$ ) appear simultaneously at  $T = T_{\text{CDW}}$ . We now show that the analysis beyond mean-field yields a preemptive instability at  $T^* > T_{\text{CDW}}$ , in which  $\Delta_1^Q$  and  $\Delta_2^Q$  condense into a “bound state” with zero total momentum. In between  $T^*$  and  $T_{\text{CDW}}$ ,  $\delta\rho(r) = j_x(r) = 0$ , but  $\Upsilon \propto \langle \delta\rho(r)j_x(r) \rangle$  becomes non-zero. Under time reversal,  $\Upsilon$  transforms into  $-\Upsilon$ , hence this order breaks time reversal symmetry. In physics terms,  $\Upsilon \neq 0$  implies that fluctuations of  $\delta\rho(r)$  and  $j_x(r)$  become correlated, i.e., this order alone generates loop currents. A center of each loop fluctuates along  $r_y$ , but a uniform magnetic field which these loop currents create is unaffected by such fluctuations and increases proportional to  $\Upsilon$ .

To verify whether the bound state develops we use the same strategy as in the analysis of a preemptive ne-

matic instability in Fe-pnictides<sup>46</sup> and apply Hubbard-Stratonovich transformation to the effective action in equation (3) by introducing collective variables  $\Upsilon \propto i(\Delta_1^Q(\Delta_2^Q)^* - (\Delta_1^Q)^*\Delta_2^Q)$  and  $\Phi \propto (|\Delta_1^Q|^2 + |\Delta_2^Q|^2)$ . Integrating over the fields  $\Delta_1^Q$  and  $\Delta_2^Q$  we obtain (see SM) the effective action in terms of collective variables  $\Upsilon$  and  $\Phi$  in the form

$$\mathcal{S}_{\text{eff}}(\Upsilon, \Phi) = \int_q \frac{\Upsilon^2}{4\beta_1} - \frac{\Phi^2}{8\beta_1} + \log[(\alpha_q + \Phi)^2 - \Upsilon^2] \quad (5)$$

where  $\int_q = T \int d^2q/(4\pi^2)$  and we included the usual  $q^2$  dispersion into the quadratic term by replacing  $\alpha$  in (3) by  $\alpha_q = \alpha + q^2$ . For simplicity, we consider only thermal fluctuations, i.e., neglect the dynamical term in  $\alpha_q$ .

We analyze  $\mathcal{S}_{\text{eff}}(\Upsilon, \Phi)$  in the saddle-point approximation, by solving the coupled set of saddle-point equations

$$\begin{aligned} \Upsilon &= 4\beta_1 \int_q \frac{\Upsilon}{(\alpha_q + \Phi)^2 - \Upsilon^2} \\ \Phi &= 8\beta_1 \int_q \frac{\alpha_q + \Phi}{(\alpha_q + \Phi)^2 - \Upsilon^2} \end{aligned} \quad (6)$$

Our goal is to verify whether a solution with  $\Upsilon \neq 0$  appears before charge order sets in. Integrating over  $q$  in (6), expressing  $\Phi$  in terms of  $\Upsilon$ , and introducing  $\Upsilon^* = \Upsilon(\pi/\beta_1)$ , we obtain from (6) the equation of  $\Upsilon^*$  in the form

$$\Upsilon^* \coth \Upsilon^* + 2 \log \frac{\Upsilon^*}{\sinh \Upsilon^*} = \alpha^* \quad (7)$$

where  $\alpha^*$  is the distance to  $T_{\text{CDW}}$ , renormalized by Gaussian fluctuations associated with the field  $\Phi$ . The charge order in this approximation emerges when  $\alpha^*$  changes sign and becomes negative. Equation (7) shows that before this happens, a non-zero solution for  $\Upsilon^*$  emerges via a second-order transition at  $\alpha^* = 1$ , i.e., at  $T = T^* > T_{\text{CDW}}$ . A non-zero  $\Upsilon^* \propto i(\Delta_1^Q(\Delta_2^Q)^* - (\Delta_1^Q)^*\Delta_2^Q)$  implies the appearance of a non-zero homogeneous ( $q = 0$ ) composite order  $i\langle \Delta_1^Q(\Delta_2^Q)^* \rangle \propto \Upsilon$ . As an independent verification, we obtained the transition at  $T^*$  by solving self-consistent equation on the “bound state”  $\langle \Delta_1^Q(\Delta_2^Q)^* \rangle$  directly from equation (3), by summing up ladder diagrams, much like it was done in the analysis of preemptive spin-current order in anisotropic triangular antiferromagnets<sup>55</sup> and in Heisenberg-Kitaev model on a hyperhoneycomb lattice<sup>56</sup> (see SM for details).

We also performed a more realistic derivation of the effective action for  $\Delta_1^Q$  and  $\Delta_2^Q$  by integrating over some finite range around hot spots and keeping the  $k$  dependence of  $\Delta_k^Q$  (i.e., not approximating it by  $\Delta_{k_0}^Q$  or  $\Delta_{k_\pi}^Q$ ). We found that the prefactors for the quadratic terms  $|\Delta_1^Q|^2$  and  $|\Delta_2^Q|^2$  in (3) are slightly different, and the instability temperature is higher for the density part  $\Delta_1^Q$ . This agrees with the consideration in Ref. [44]. In the mean-field description this would imply that the system develops only a stripe density modulation, but no

current. However, beyond mean-field theory, the bound state still develops at  $T^*$ , and forces  $\Delta_2^Q$  and  $\Delta_1^Q$  to order simultaneously at  $T_{CDW}$ , as long as  $T^* - T_{CDW}$  exceeds the difference between the mean-field transition temperatures for  $\Delta_1^Q$  and  $\Delta_2^Q$ .

### III. THE PHASE DIAGRAM AND THE RELATION TO THE EXPERIMENTS

To construct the phase diagram, we first consider how  $T_{CDW}(\xi)$  evolves when hole doping increases and magnetic correlation length decreases. We found that at a finite  $\xi$ , the scale  $v_F^2 \xi^{-2} / \bar{g} \sim \bar{g} / \lambda^2$  serves as the lower energy cut-off for the logarithm, i.e.,  $T$  in (1) gets replaced by  $(T^2 + \bar{g}^2 / \lambda^4)^{1/2}$ . As the consequence,  $T_{CDW}(\xi)$  decreases with increasing  $\xi$  and vanishes when  $\xi_{cr}^{-1} \sim \bar{g} / v_F$ , i.e. when the dimensionless coupling constant  $\lambda \sim 1$ . We show this behavior in Fig. 1(b). The vanishing of  $T_{CDW}(\xi_{cr})$  sets up a charge QCP at some distance away from a magnetic QCP. The temperature  $T^*$  at which composite order sets in also gets smaller as  $\xi$  increases. We analyzed the emergence of the composite and CDW orders at  $T = 0$  using the same approach as in Ref. 45 (this requires one to include the dynamical term into  $\alpha_q$  in equation (5)) and found that the two orders emerge simultaneously via a weak first-order transition. We show the behavior of  $T_{CDW}(\xi)$  and  $T^*(\xi)$  in Fig. 3(b).

Panels (a) and (b) in Fig. 3 show the onset temperatures for CDW and composite order and for SC order, when the two are considered independent on each other. In reality, charge and SC orders compete for hot fermions on the FS, and the competition implies that the order, which sets up first, tend to suppress the other one. In the spin-fluctuation approach, the value of  $T_c$  is larger than  $T_{CDW}$ , but the two are of the same order and comparable in magnitude (see SM). The value of  $T^*$  is larger than  $T_{CDW}$ , and we assume that at large  $\xi$ ,  $T^* > T_c$ , i.e., the composite charge order sets up first upon the lowering of  $T$ . The composite order suppresses  $T_c$  and gives rise to a non-monotonic behavior of  $T_c(\xi)$  already in the paramagnetic phase. At the same time, it increases the correlation length for the primary CDW order parameter<sup>46</sup>, i.e, the composite order tends to increase  $T_{CDW}$ . At large  $\xi$ ,  $T_{CDW}$  then well may become larger than the reduced  $T_c$ , in which case charge order develops prior to superconductivity. At the lowest  $T$ , CDW and SC orders can either be separated by a first order transition or co-exist, with co-existence more likely due to, e.g., a close analogy of our case with the one for Fe-pnictides, where co-existence has been verified in microscopic calculations<sup>48,49</sup>. The corresponding phase diagram is shown in Fig. 3(c). It has a number of features consistent with the experimental data on hole-doped cuprates.

We performed a more detailed comparison with the ARPES data. The data show two major changes in the spectral function upon lowering of  $T$  as the system enters into the regime of strong CDW fluctuations First, upon

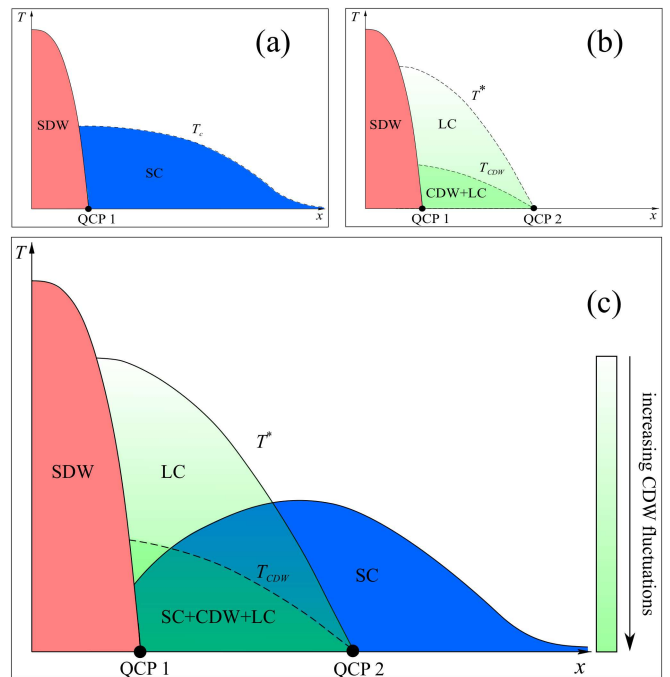


FIG. 3: Panels (a) and (b) – the behavior of superconducting  $T_c$  (panel a) and the onset temperatures for charge order  $T^*$  and  $T_{CDW}$  (panel b), when SC and charge ordered are treated independent on each other. Panel (c) – the phase diagram, which includes the competition between SC and charge order. LC stands for “loop currents”, by which we specifically mean a  $q = 0$  order which breaks time-reversal symmetry. QCP<sub>1</sub> and QCP<sub>2</sub> are quantum-critical points towards SDW order and charge order, respectively.

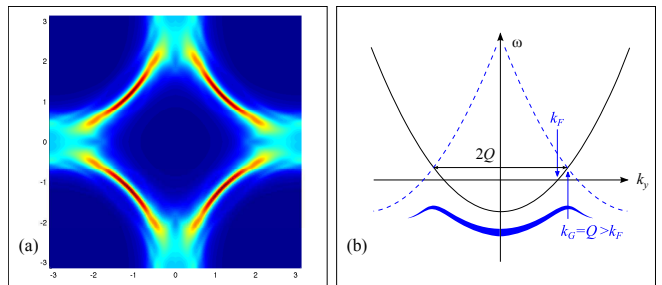


FIG. 4: The theoretical spectral function for a state with strong CDW fluctuations, which we model by introducing CDW orders  $\Delta_x$  and  $\Delta_y$ , but keeping a finite lifetime of fermions on the FS. Panel (a) – the spectral function at  $\omega = 0$ . Fermi arcs are clearly visible. Panel (b) – the dispersion along  $(k_x, \pi)$  line near  $k_x = 0$ . The minimum of dispersion shifts from  $k_F$  to  $k_G > k_F$ , in agreement with the data in [20].

crossing  $T^*$ , the spectral weight in the antinodal regions transforms to higher frequencies, leading to Fermi arcs<sup>57</sup>. Second, careful measurements of the spectral function in  $\text{Pb}_{0.55}\text{Bi}_{1.5}\text{Sr}_{1.6}\text{La}_{0.4}\text{CuO}_{6+\delta}$  along  $(k_x, \pi)$  line in the Brillouin zone showed<sup>20</sup> that the minimum of the dispersion shifts from  $k_F$  to  $k_G > k_F$  (the blue line in Fig. 4(b)). One should not expect such a shift if the pseudo-

gap was a precursor to superconductivity, and if the pseudogap was a precursor to magnetism (or to CDW order with a diagonal  $Q$ ), the shift would be in opposite direction. These two features are reproduced in our theory. We model the state without CDW order but with strong CDW fluctuations by introducing a CDW condensate but keeping a finite lifetime of fermions near the FS. We also assume that there are domains of CDW/composite order along both  $x$  and  $y$  directions, and ARPES measures contributions from both domains. We present the details of the analysis in the SM, including the analysis of additional changes in ARPES upon entering into the SC state, and show the two key results in Fig. 4. Fig. 4a shows the spectral weight along the original FS. The arcs are clearly visible. In Fig. 4(b) we show the quasi-particle dispersion at along  $(k_x, \pi)$  direction. We argue that this dispersion gets modified primarily by mixing up the states with  $\mathbf{k}$  and  $\mathbf{k} + \mathbf{Q}_x$ , where, we remind,  $\mathbf{Q}_x = (2Q, 0)$ . Because  $2Q$  is larger than the distance  $2k_F$  between FS points along  $(k_x, \pi)$ , the crossing of  $\epsilon_{\mathbf{k}}$  and  $\epsilon_{\mathbf{k}+2\mathbf{Q}_x}$  (solid and dashed lines in Fig. 4b) necessary occurs at  $k_G = Q > k_F$ , and this  $k_G$  becomes the minimum of the dispersion once CDW order develops. This agrees with the data in [20].

#### IV. OUTLOOK

The goal of this paper was two-fold. First, to understand whether spin-fluctuation approach, which describes  $d$ -wave superconductivity and non-FI physics in the normal state, also allows one to understand the pseudogap physics in hole-doped cuprates. Second, to study the structure of charge order parameter and potential preemptive instability which breaks a discrete time-reversal symmetry but leaves a continuous translational symmetry intact. We argued that magnetically-mediated interaction gives rise to charge order with momenta  $Q_x = (2Q, 0)$  and  $Q_y = (0, 2Q)$ , as seen in the experiments. The critical temperature for the onset of the charge order  $T_{\text{CDW}}$  is comparable to  $T_c$  at large values of magnetic correlation length  $\xi$ , but terminates at  $T = 0$  at some finite doping  $\xi$ , setting up the second quantum critical point at some distance away from the

magnetic one. We show that the emerging charge order is of stripe type – it appears with either  $Q_x$  or  $Q_y$ , but not with both.

Our most significant observation is that CDW order parameter with, say,  $Q_y$  has two components: one is incommensurate density variation  $\delta\rho(r) \propto \cos 2Qy$ , another is incommensurate current  $j_x(r) \propto \sin 2Qy$ . In mean-field approximation, both appear below  $T_{\text{CDW}}$ , and the resulting CDW state breaks lattice translational and rotational symmetries and time-reversal symmetry, and generates a uniform orbital magnetic field. We performed calculations beyond mean-field and found that time-reversal symmetry gets broken at  $T^* > T_{\text{CDW}}$ . In between  $T^*$  and  $T_{\text{CDW}}$ , both density and current components fluctuate, such that  $\langle \delta\rho(r) \rangle = \langle j_x(r) \rangle = 0$ , however their fluctuations are correlated, and the composite order  $\langle \delta\rho(r)j_x(r) \rangle$  is non-zero. Such an order breaks time-reversal symmetry and generates loop currents, however lattice symmetries remain unbroken.

The phase diagram resulting from our analysis is shown in Fig. 3c. It has numerous features consistent with the experiments on hole-doped cuprates. We performed a more detailed comparison with ARPES studies and found good quantitative agreement with the data. Overall, we believe that the most significant result of our theory is that it shows that pseudogap physics can be well understood within the same spin-fermion model which was earlier shown to yield  $d$ -wave superconductivity and non-Fermi liquid physics. We believe that, with our result, the spin-fermion model re-emerges as the strong candidate for the theoretical model for the cuprates.

One issue left for further study is the interplay between the preemptive transition, which breaks time-reversal symmetry, and potential preemptive nematic transition, which breaks the symmetry between  $x$  and  $y$  direction before the true CDW order sets in. Such a transition (similar to the one in Fe-pnictides<sup>45</sup> has been recently argued to develop in the cuprates at  $T > T_{\text{CDW}}$  in the presence of quenched disorder<sup>58</sup>. Another issue for further study is to what extent CDW order and preemptive transitions vary between different families of hole-doped the cuprates. And the third one is the relation between our current loop order and neutron scattering results from Refs. [2,3].

<sup>1</sup> He, R.-H. *et al.*, From a single-band metal to a high-temperature superconductor via two thermal phase transitions, *Science* **331**, 1579 (2011).

<sup>2</sup> for the latest review see Sidis, Y. & Bourges, P. Evidence for intra-unit-cell magnetic order in the pseudo-gap state of high- $T_c$  cuprates, arXiv:1306.5124.

<sup>3</sup> Li, Y. *et al.* Hidden magnetic excitation in the pseudogap phase of a model cuprate superconductor. *Nature* **468**, 283 (2010).

<sup>4</sup> Karapetyan, H. *et al.* Magneto-Optical Measurements of a Cascade of Transitions in Superconducting

$\text{La}_{1.875}\text{Ba}_{0.125}\text{CuO}_4$  Single Crystals. *Phys. Rev. Lett.* **109**, 147001 (2012) and references therein

<sup>5</sup> Hosur, P., Kapitulnik, A., Kivelson, A. S., Orenstein, J., & Raghu, S. Kerr effect as evidence of gyrotropic order in the cuprates. *Phys. Rev. B* **87**, 115116 (2013).

<sup>6</sup> Hücker, M. *et al.* Stripe order in superconducting  $\text{La}_{2-x}\text{Ba}_x\text{CuO}_4$  ( $0.095 \leq x \leq 0.155$ ). *Phys. Rev. B* **83**, 104506 (2011).

<sup>7</sup> Tranquada, J. M. *et al.* Evidence for unusual superconducting correlations coexisting with stripe order in  $\text{La}_{1.875}\text{Ba}_{0.125}\text{CuO}_4$ . *Phys. Rev. B* **78**, 174529 (2008).

- <sup>8</sup> Hinkov, V. *et al.* Spin dynamics in the pseudogap state of a high-temperature superconductor. *Nat. Phys.* **3**, 780 (2007).
- <sup>9</sup> Fujita, K. *et al.* Spectroscopic Imaging Scanning Tunneling Microscopy Studies of Electronic Structure in the Superconducting and Pseudogap Phases of Cuprate High-Tc Superconductors. *J. Phys. Soc. Jpn.* **81**, (2012) 011005.
- <sup>10</sup> LeBoeuf, D. *et al.* Thermodynamic phase diagram of static charge order in underdoped YBCO. *Nat. Phys.* **9**, 79 (2013).
- <sup>11</sup> Wu, T. *et al.* Magnetic-field-induced charge-stripe order in the high-temperature superconductor  $\text{YBa}_2\text{Cu}_3\text{O}_y$ . *Nature* **477**, 191-194 (2011).
- <sup>12</sup> Wu, T. *et al.* Emergence of charge order from the vortex state of a high-temperature superconductor. *Nat. Commun.*, **4** 2113 (2013).
- <sup>13</sup> Meier, H., Eimenkel, M., Pepin, C., & Efetov, K. B. Effect of magnetic field on competition between superconductivity and charge order below the pseudogap state. *Phys. Rev. B* **88**, 020506(R) (2013).
- <sup>14</sup> Ghiringhelli, G. *et al.* Long-range incommensurate charge fluctuations in  $(\text{Y,Nd})\text{Ba}_2\text{Cu}_3\text{O}_{6+\delta}$ . *Science* **337**, 821 (2012).
- <sup>15</sup> Achkar, A. J. *et al.* Distinct charge orders in the planes and chains of ortho-III ordered  $\text{YBa}_2\text{Cu}_3\text{O}_{6+\delta}$  identified by resonant ray scattering. arXiv:1207.3667, (2012).
- <sup>16</sup> Comin, X.-R. *et al.* Charge order driven by Fermi-arc instability in  $\text{Bi}_2\text{Sr}_x\text{La}_x\text{CuO}_{6+\delta}$ . arXiv:1312.1343.
- <sup>17</sup> da Silva Neto, E.-H. *et al.* Ubiquitous interplay between charge ordering and high-temperature superconductivity in cuprates. arXiv:1312.1347.
- <sup>18</sup> Harrison, N. & Sebastian, S. E. Protected Nodal Electron Pocket from Multiple-Q Ordering in Underdoped High Temperature Superconductors. *Phys. Rev. Lett.* **106**, 226402 (2011).
- <sup>19</sup> Doiron-Leyraud, N. & Taillefer, L. Quantum critical point for stripe order: an organizing principle of cuprate superconductivity. *Physica C* **481**, 161 (2012).
- <sup>20</sup> Vishik, I. M. *et al.* Phase competition in trisected superconducting dome. *Proc. Natl. Acad. Sci. USA* **110**, 17774 (2013).
- <sup>21</sup> Basov, D. N., Averitt, R. D., van der Marel, D., Dressel, M., & Haule, K. Electrodynamics of correlated electron materials. *Rev. Mod. Phys.* **83**, 471 (2011).
- <sup>22</sup> Henri, A. What is the simplest model which captures the basic experimental facts of the physics of underdoped cuprates? arXiv:1302.3473
- <sup>23</sup> Scalapino, D. J. A common thread: The pairing interaction for unconventional superconductors. *Rev. Mod. Phys.* **84**, 1383 (2012).
- <sup>24</sup> Monthoux, P., Pines, D., & Lonzarich, G. G. Superconductivity without phonons. *Nature* **450**, 1177-1183 (2007)
- <sup>25</sup> Abanov, Ar. Chubukov, A. V. & Finkelstein, M. A. Coherent vs. incoherent pairing in 2D systems near magnetic instability. *Europhys. Lett.* **54**, 488 (2001).
- <sup>26</sup> Abanov, Ar. Chubukov, A. V. & Schmalian, J. Quantum-critical theory of the spin fermion model and its application to cuprates: normal state analysis. *Adv. Phys.* **52**, 119 (2003).
- <sup>27</sup> Hartnoll, S. A., Hofman, D. M., Metlitski, M. A., & Sachdev, S. Quantum critical response at the onset of spin-density-wave order in two-dimensional metals. *Phys. Rev. B* **84**, 125115 (2011).
- <sup>28</sup> Varma, C. M., Non-Fermi-liquid states and pairing instability of a general model of copper oxide metals. *Phys. Rev. B* **55** 14554 (1997).
- <sup>29</sup> Wang, Z., Kotliar, G., & Wang, X.-F. Flux-density wave and superconducting instability of the staggered-flux phase. *Phys. Rev. B* **42**, 8690 (1990).
- <sup>30</sup> Chakravarty, S., Laughlin, R. B., Morr, D. K. & Nayak, C. Hidden order in the cuprates. *Phys. Rev. B* **63**, 094503 (2001).
- <sup>31</sup> Lee, P. A., Nagaosa, N., & Wen, X.-G. Doping a Mott insulator: Physics of high-temperature superconductivity. *Rev. Mod. Phys.* **78**, 17 (2006).
- <sup>32</sup> Gull, E., Parcollet, O., & Millis, A. J. Superconductivity and the Pseudogap in the two-dimensional Hubbard model. *Phys. Rev. Lett.* **110**, 216405 (2013).
- <sup>33</sup> Tremblay, A.-M. S. Strongly correlated superconductivity. arXiv:1310.1481.
- <sup>34</sup> Choy T.-P. & Phillips Ph. Doped Mott Insulators Are Insulators: Hole Localization in the Cuprates *Phys. Rev. Lett.* **95**, 196405 (2005).
- <sup>35</sup> Rice, T. M., Yang, K.-Y. & Zhang, F. C., A Phenomenological Theory of the Anomalous Pseudogap Phase in Underdoped Cuprates *Rep. Prog. Phys.* **75**, 016502 (2012).
- <sup>36</sup> Kyung, D.-B. *et al.* Pseudogap induced by short-range spin correlations in a doped Mott insulator. *Phys. Rev. B* **73**, 165114 (2006).
- <sup>37</sup> Schmalian, J., Pines, D., & Stojkovich, B. Weak Pseudogap Behavior in the Underdoped Cuprate Superconductors. *Phys. Rev. Lett.* **80**, 3839 (1998).
- <sup>38</sup> Sedrakyan, T. A. & Chubukov, A. V. Pseudogap in underdoped cuprates and spin-density-wave fluctuations. *Phys. Rev. B* **81**, 174536 (2010).
- <sup>39</sup> Emery, V. J. & Kivelson, A. S. Importance of phase fluctuations in superconductors with small superfluid density. *Nature* **374**, 434 (1994).
- <sup>40</sup> Benfatto, L. *et al.* Phase fluctuations, dissipation, and superfluid stiffness in wave superconductors. *Phys. Rev. B* **63**, 174513 (2001).
- <sup>41</sup> Metlitski, M. A. & Sachdev, S. Quantum phase transitions of metals in two spatial dimensions: II. Spin density wave order. *Phys. Rev. B* **82**, 075128 (2010).
- <sup>42</sup> Efetov, K. B., Meier, H., & Pépin, C. Pseudogap state near a quantum critical point. *Nat. Phys.* **9** 442, (2013)
- <sup>43</sup> Hayward, L. E., Hawthorn, D. G., Melko, R. G., & Sachdev, S. Angular fluctuations of a multi-component order describe the pseudogap regime of the cuprate superconductors, arXiv:1309.6639.
- <sup>44</sup> Sachdev, S. & La Placa, R. Bond Order in Two-Dimensional Metals with Antiferromagnetic Exchange Interactions. *Phys. Rev. Lett.* **111**, 027202 (2013).
- <sup>45</sup> Fernandes, R. M., Maiti, S., Wölfle, P., & Chubukov, A. V. How many quantum phase transitions exist inside the superconducting dome of the iron pnictides? *Phys. Rev. Lett.*, **111**, 057001 (2013).
- <sup>46</sup> Fernandes, R. M., Chubukov, A. V., Knolle, J., Eremin, I., & Schmalian, J. Preemptive nematic order, pseudogap, and orbital order in the iron pnictides. *Phys. Rev. B* **85**, 024534 (2012).
- <sup>47</sup> Meier, H., Pépin, C., Eimenkel, M., & Efetov, K. B. Cascade of phase transitions in the vicinity of a quantum critical point arXiv:1312.2010.
- <sup>48</sup> Vorontsov, B. A., Vavilov, M. G., & Chubukov, A. V. Superconductivity and spin-density waves in multiband metals. *Phys. Rev. B* **81**, 174538 (2010)
- <sup>49</sup> Fernandes, R. M. & Schmalian, J. Competing order and



- nature of the pairing state in the iron pnictides. *Phys. Rev. B* **82**, 014521 (2010).
- <sup>50</sup> Wang, Y. & Chubukov, A. Superconductivity at the onset of the spin-density-wave order in a metal. *Phys. Rev. Lett.* **110**, 127001 (2013).
- <sup>51</sup> Abanov, Ar., Chubukov, A. V., & Norman, M. R. Gap anisotropy and universal pairing scale in a spin-fluctuation model of cuprate superconductors. *Phys. Rev. B* **78**, 220507(R) (2008).
- <sup>52</sup> see e.g., Berg, E., Fradkin, E., Kivelson, S. A. & Trnquada, J. Striped superconductors: How the cuprates intertwine spin, charge and superconducting orders *New J. Phys.* **11**, 115004 (2009).
- <sup>53</sup> Tewari, S., Zhang, C., Yakovenko, V. M., & Das Sarma, S. Time-Reversal Symmetry Breaking by a  $(d + id)$  Density-Wave State in Underdoped Cuprate Superconductors. *Phys. Rev. Lett.* **100**, 217004 (2008).
- <sup>54</sup> Hsu, C.-H., Raghu, S., & Chakravarty, S. Topological density wave states of nonzero angular momentum. *Phys. Rev. B* **84**, 155111 (2011).
- <sup>55</sup> Chubukov, A. V. & Starykh, O. A. Spin-Current Order in Anisotropic Triangular Antiferromagnets. *Phys. Rev. Lett.* **110**, 217210 (2013).
- <sup>56</sup> Dhar, A. *et al.* Chiral Mott insulator with staggered loop currents in the fully frustrated Bose-Hubbard model. *Phys. Rev. B* **87**, 174501 (2013).
- <sup>57</sup> Norman, M. R. *et al.* Destruction of the Fermi surface in underdoped high- $T_c$  superconductors. *Nature* **392**, 157 (1998).
- <sup>58</sup> Nie, L., Tarjus, G., & Kivelson, S. A., Quenched disorder and vestigial nematicity in the pseudo-gap regime of the cuprates, arXiv:1311.5580 (2013).

## Acknowledgments

We thank Ar. Abanov, H. Alloul, D. Basov, Ph. Bourges, K. Efetov, R. Fernandes, P. Goswami, M-H. Julien, H. Maier, E. Mishchenko, B. Keimer, S. Kivelson, M. Norman, A. Paramakanti, C. Pépin, D. Pesin, N. Perkins, J. Schmalian, D. Scalapino, S. Sebastian, and O. Starykh for fruitful discussions. The work was supported by the DOE grant DE-FG02-ER46900.

---

## SUPPLEMENTARY MATERIAL

### V. A SET OF LINEARIZED EQUATIONS FOR CDW ORDER PARAMETER WITH MOMENTUM $(2Q, 0)$ OR $(0, 2Q)$

#### A. Linearized gap equation to a logarithmic accuracy

In this section we present the details of the derivation of the linearized equation for the CDW order parameters  $\Delta_{\mathbf{k}}^Q = \langle c_{k+Q}^\dagger c_{k-Q} \rangle$  and  $\Delta_{\mathbf{k}+\pi}^Q$  with momentum  $\mathbf{Q}$  along either  $x$  or  $y$  axis, at the onset of SDW order, when the magnetic correlation length  $\xi$  is infinite. Solving these equations we obtain  $T_{\text{CDW}}(\xi = \infty)$ . We later consider how  $T_{\text{CDW}}(\xi)$  evolves when  $\xi$  decreases. Borrowing notations from superconductivity, we will be calling the equations for  $\Delta_{\mathbf{k}}^Q$  and  $\Delta_{\mathbf{k}+\pi}^Q$  as “gap” equations.

We first solve the set of coupled linearized gap equations to logarithmic accuracy and show that the kernel is logarithmically singular at  $T = 0$  and favors the solution with opposite signs of  $\Delta_{\mathbf{k}}^Q$  and  $\Delta_{\mathbf{k}+\pi}^Q$ . Then we consider the full solution for frequency-dependent CDW order parameters and show that logarithmic accuracy is not sufficient because a formal summation of the leading logarithms does not lead to an instability. This is rather typical situation for the instability at a quantum-critical point (QCP), when the “pairing boson” is massless (see e.g., Ref. [1]). We solve for the CDW instability beyond the logarithmic approximation and show that this is a threshold problem, i.e., the CDW instability emerges only if the effective coupling constant exceeds a threshold value. For the quantum-critical problem that we consider, the effective coupling is a universal number of order one, and we verify that its value is above the threshold. As a result, a CDW instability does develop at a certain finite  $T_{\text{CDW}}$ .

As Fig. 5 shows, the CDW order parameters at  $k_0$  and  $k_\pi \equiv k_0 + (\pi, \pi)$  are expressed via each other, and one needs to solve a set of two coupled gap equations to find an instability. Each equation is, in general, an integral equation in both frequency and momentum. Besides, fermionic propagators in the r.h.s. of the gap equations contain the self-energy  $\Sigma(k, \Omega_m)$  which is (i) not small and (ii) depends on frequency  $\Omega_m$  and also on the deviation of an internal fermion from a corresponding hot spot along the Fermi surface (FS) (Refs. [2,3]). For simplicity, we will keep only frequency dependence in the fermionic self-energy and in the gap functions, i.e., approximate  $\Sigma(k, \Omega_m) \approx \Sigma(k_h, \Omega_m) \equiv \Sigma_{\Omega_m}$ ,  $\Delta_k^Q(\Omega_m) \approx \Delta_{k_0}^Q(\Omega_m)$  when  $k$  is near  $k_0$ , and  $\Delta_k^Q(\Omega_m) \approx \Delta_{k_\pi}^Q(\Omega_m)$  when  $k$  is near  $k_\pi$ . Such an approximation has been verified [4] to be a valid one near a superconducting instability, and we expect it to be valid also for a CDW transition.

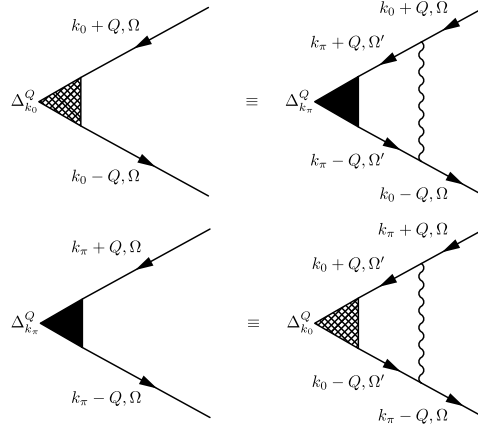


FIG. 5: The set of linearized equations for CDW vertices constructed out of fermions near hot spots. The momenta  $k_0$  and  $k_\pi = k_0 + (\pi, \pi)$  are in between the two neighboring hot spots either along  $x$  or along  $y$  direction, chosen such that  $k_0 \pm Q$  and  $k_\pi \pm Q$  are right at the hot spots. The solid lines are full fermionic propagators, the wavy lines represent spin-mediated interaction peaked at  $(\pi, \pi)$ .

The set of the two integral equations in frequency for  $\Delta_{k_0}^Q(\Omega_m)$  and  $\Delta_{k_\pi}^Q(\Omega_m)$  has the form

$$\Delta_{k_0}^Q(\Omega_m) = \frac{3\bar{g}T}{4\pi^2} \sum_{m'} \int \frac{dx dy}{[i\Sigma_{\Omega_{m'}} - v_x y + v_y x] [i\Sigma_{\Omega_{m'}} + v_x y + v_y x]} \frac{\Delta_{k_\pi}^Q(\Omega_{m'})}{x^2 + y^2 + \gamma|\Omega_m - \Omega_{m'}|} \quad (8)$$

$$\Delta_{k_\pi}^Q(\Omega_m) = \frac{3\bar{g}T}{4\pi^2} \sum_{m'} \int \frac{dx dy}{[i\Sigma_{\Omega_{m'}} - v_x x + v_y y] [i\Sigma_{\Omega_{m'}} - v_x x - v_y y]} \frac{\Delta_{k_0}^Q(\Omega_{m'})}{x^2 + y^2 + \gamma|\Omega_m - \Omega_{m'}|}, \quad (9)$$

where  $\gamma = 4\bar{g}/(\pi(v_y^2 - v_x^2))$ ,  $x$  and  $y$  are momentum deviations from the corresponding hot spots, and

$$\Sigma_{\Omega_{m'}} \equiv \Omega_{m'} + \Sigma(\Omega_{m'}) = \text{sgn}(\Omega_{m'}) \sqrt{\omega_0 |\Omega_{m'}|} \left( 1 + \sqrt{\frac{|\Omega_{m'}|}{\omega_0}} \right), \quad (10)$$

where  $\omega_0 = 9\bar{g}/(16\pi) \times [(v_y^2 - v_x^2)/v_F^2]$  (Ref. [2]). By order of magnitude,  $\omega_0$  coincides with the spin-fermion coupling constant  $\bar{g}$ . We choose  $k_0$  to be near  $(0, \pi)$  in Fig. 1 in the main text, in which case  $v_x < v_y$ .

We first integrate over  $x$  in Eq. (8) and obtain,

$$\Delta_{k_0}^Q(\Omega_m) = \frac{3\bar{g}T}{8\pi} \sum_{m'} \int_0^\infty \frac{dy}{\sqrt{y^2 + \gamma|\Omega_m - \Omega_{m'}|}} \frac{\Delta_{k_\pi}^Q(\Omega_{m'})}{v_x^2 y^2 + (v_y \sqrt{y^2 + \gamma|\Omega_m - \Omega_{m'}|} + \Sigma_{\Omega_{m'}})^2}. \quad (11)$$

Introducing then  $z = y/\sqrt{\gamma|\Omega_{m'}|}$  and  $\varphi = \arctan(v_x/v_y)$  we obtain from (11)

$$\begin{aligned} \Delta_{k_0}^Q(\Omega_m) &= -\frac{3 \cos 2\varphi}{16\pi} \int \frac{d\Omega_{m'}}{|\Omega_{m'}|} \frac{\Delta_{k_\pi}^Q(\Omega_{m'})}{\sqrt{z^2 + |1 - \Omega_{m'}/\Omega_m|}} \\ &\times \frac{1}{z^2 \sin^2 \varphi + [\sqrt{z^2 + |1 - \Omega_{m'}/\Omega_m|} \cos \varphi + 3/8 \cos 2\varphi (1 + \sqrt{\Omega_{m'}/\omega_0})]^2}. \end{aligned} \quad (12)$$

Following similar steps, we find

$$\begin{aligned} \Delta_{k_\pi}^Q(\Omega_m) &= -\frac{3 \cos 2\varphi}{16\pi} \int \frac{d\Omega_{m'}}{|\Omega_{m'}|} \frac{\Delta_{k_0}^Q(\Omega_{m'})}{\sqrt{z^2 + |1 - \Omega_{m'}/\Omega_m|}} \\ &\times \frac{1}{z^2 \cos^2 \varphi + [\sqrt{z^2 + |1 - \Omega_{m'}/\Omega_m|} \sin \varphi + 3/8 \cos 2\varphi (1 + \sqrt{\Omega_{m'}/\omega_0})]^2}. \end{aligned} \quad (13)$$

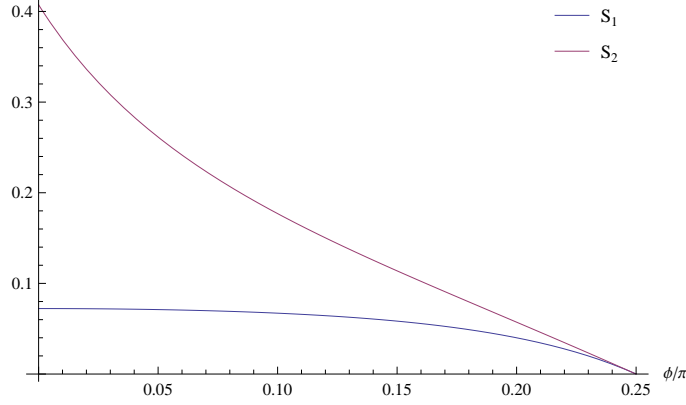


FIG. 6: The integrals  $S_1$  and  $S_2$  as functions of the angle  $\varphi$ . Both integrals vanish at  $\varphi = \pi/4$  because at this  $\varphi$  the Landau damping coefficient diverges.

The value of  $\varphi$  depends on the geometry of the FS. When Fermi velocities at hot spots 1 and 2 in Fig. 1 in the main text are nearly antiparallel, and the ones at hot spots 3 and 4 are nearly parallel, we have  $\varphi \approx 0$ . When Fermi velocities at hot spots 1 and 2 are nearly perpendicular to each other, we have  $\varphi \approx \pi/4$ . For the FS as in hole-doped cuprates,  $\varphi$  is non-zero, but definitely smaller than  $\pi/4$ .

The negative signs in the right hand sides of (12) and (13) imply that the solution is only possible when  $\Delta_{k_0}^Q(\Omega_m)$  and  $\Delta_{k_\pi}^Q(\Omega_m)$  have opposite signs, i.e., CDW order parameter  $\Delta_k^Q(\Omega_m)$  changes sign under  $\mathbf{k} \rightarrow \mathbf{k} + (\pi, \pi)$ . This does not imply, however, that CDW order is a bond order<sup>3</sup>,  $\langle c^\dagger(r+a)c(r) \rangle$ , with no on-site component  $\langle c^\dagger(r)c(r) \rangle$ . In our case,  $\Delta_{k_0}^Q(\Omega_m)$  and  $\Delta_{k_\pi}^Q(\Omega_m)$  differ in magnitude, hence, if CDW order emerges, it gives rise to both on-site and bond components.

As a first pass on Eqs. (12) and (13), we approximate gap functions as frequency-independent constants and set the lower limit of integration over internal fermionic frequency to  $\pi T$ . Evaluating the integrals with two fermionic and one bosonic propagators, we find that they are logarithmically singular, no matter what  $\varphi$  is. We obtain

$$\begin{aligned}\Delta_{k_0}^Q &= -S_1(\varphi) \log \frac{\omega_0}{T} \Delta_{k_\pi}^Q, \\ \Delta_{k_\pi}^Q &= -S_2(\varphi) \log \frac{\omega_0}{T} \Delta_{k_0}^Q.\end{aligned}\quad (14)$$

where

$$\begin{aligned}S_1(\varphi) &= \frac{3 \cos 2\varphi}{8\pi} \int_0^\infty \frac{dz}{\sqrt{z^2+1}} \frac{1}{z^2 \sin^2 \varphi + (\sqrt{z^2+1} \cos \varphi + 3/8 \cos 2\varphi)^2} \\ S_2(\varphi) &= \frac{3 \cos 2\varphi}{8\pi} \int_0^\infty \frac{dz}{\sqrt{z^2+1}} \frac{1}{z^2 \cos^2 \varphi + (\sqrt{z^2+1} \sin \varphi + 3/8 \cos 2\varphi)^2}.\end{aligned}\quad (15)$$

This is the result which we cited in Eq. (1) in the main text. We emphasize that these two functions remain finite even if we set  $\varphi = 0$ . For  $S_2$ , this is an expected result as in this limit the velocities of hot fermions 1 and 2 in Fig. 1 of the main text are anti-parallel, and the kernel in CDW channel is essentially the same as in the superconducting channel. For  $S_1$ , this is a less expected result as the velocities of hot fermions 3 and 4 in Fig. 1 of the main text become parallel for  $\varphi = 0$ . On a more careful look, we found that in this case the integral is non-zero because of the presence of a branch cut in the Landau damping term in the bosonic propagator.

Evaluating  $S_1$  and  $S_2$  numerically, we found (see Fig. 6) that  $S_2 > S_1 > 0$  as long as  $\varphi < \pi/4$ . That  $S_2 > S_1$  implies that the CDW order parameter in the region with nearly antiparallel Fermi velocities (region 1-2 in our case) is smaller than in the region with nearly parallel velocities (region 3-4 in our case).

Solving the set (14) we immediately obtain a CDW instability at  $\xi = \infty$  at  $T_{\text{CDW}} \sim \omega_0 e^{-1/\sqrt{S_1 S_2}}$ . This  $T_{\text{CDW}}$  is of the same order of magnitude as superconducting  $T_c$ , which at the onset of SDW order is also of order  $\omega_0$  (Refs. [1,4]).

## B. The solution of the set of integral gap equations in frequency

Eq. (14) is an approximate result. For a more accurate treatment, we need to keep the frequency dependence in  $\Delta_{k_0}^Q(\Omega_m)$  and  $\Delta_{k_\pi}^Q(\Omega_m)$ .

Plugging Eq. (13) into Eq.(12) we get rid of  $\Delta_{k_\pi}^Q(\Omega_m)$  and obtain integral equation for  $\Delta_{k_0}^Q(\Omega)$  in the form,

$$\Delta_{k_0}^Q(\Omega_m) = T \sum_{m'} I(\Omega_m, \Omega_{m'}) \Delta_{k_0}^Q(\Omega_{m'}), \quad (16)$$

where  $I(\Omega_m, \Omega_{m'})$  is the kernel which depends on both external and internal frequencies. The strategy of perturbation theory is to add the source term  $\Delta_0$  to the right hand side of Eq. (16) and to search for the divergence of  $\Delta_{k_0}^Q/\Delta_0$  at  $T = T_{\text{CDW}}$ . At first order of perturbation theory, we replace  $\Delta_{k_0}^Q(\Omega_{m'})$  by  $\Delta_0$  in the integral part and obtain  $\Delta_{k_0}^Q(\Omega_m = \pi T) = \Delta_0(1 + \frac{1}{2}S_1S_2 \log^2 \frac{\omega_0}{T})$ . This is the same result as we had before, except for the additional 1/2 factor which is due to the requirement that, when we compute  $\sum_{m'} I(\Omega_m, \Omega_{m'})$ , the internal frequency must be much larger than the external one in order to obtain  $\log^2$  correction. However, once we include higher orders in perturbation theory and sum up the logarithms, we find that the series of  $\log^2$  terms sum up into a power-law form  $\Delta_{k_0}^Q = \Delta_0 \cosh(\sqrt{S_1S_2} \log \frac{\omega_0}{T}) \sim \Delta_0 (\frac{\omega_0}{T})^{\sqrt{S_1S_2}}$ . The ratio  $\Delta_{k_0}^Q/\Delta_0$  does not diverge at any finite  $T$ , and the implication is that the summation of the logarithmical terms does not give rise to a CDW instability. A similar situation holds in the superconducting channel. There, previous works have found<sup>1,4,5</sup> that the instability does develop, but to detect it one has to go beyond logarithmic accuracy and solve the full integral equation in frequency.

The way it works for superconducting problem is the following. An integral equation in frequency for a superconducting vertex yields a power-law solution,  $\Omega^{-\alpha}$ . When the coupling is below the threshold,  $\alpha$  is real, and the full solution is the same as one obtains in the perturbation theory by summing up the logarithms. When the coupling exceeds the threshold,  $\alpha$  becomes complex, and two solutions appear, one with  $\alpha$ , another with  $\alpha^*$ . The linear combination of these two solutions yields  $\Delta_{k_0}^Q \propto \cos[\text{Im}(\alpha) \log \omega + \theta]$  with a ‘‘free’’ phase variable  $\theta$ . The power-law behavior exists in the frequency range between  $\omega_0$  and  $T$  and has to satisfy boundary conditions at the two edges. This requires two adjustable parameters. The temperature is one of them, the phase  $\theta$  is the other one. Solving for the boundary conditions one then finds<sup>4</sup> that at some  $T = T_c$  the solution of the gap equation becomes possible even when the bare value of gap is set to zero. Note that for a real  $\alpha$ , there is no free phase factor, and boundary conditions can not be satisfied at both ends. From this perspective, the existence of a complex  $\alpha$  is the necessary conditions for the existence of SC instability in a quantum-critical regime.

We followed the same strategy for the CDW case. We kept the frequency dependencies of  $\Delta_{k_0}^Q$  and  $\Delta_{k_\pi}^Q$  in Eqs. (12) and (13), solved these two equations as integral equations, searched for a power-law solution, and analyzed when the exponent becomes complex. To shorten the presentation, we only consider the limiting case  $\varphi = 0$ , and replace the soft upper cutoff at  $\omega_0$  with a hard one. With this simplification, we obtain

$$\Delta_{k_0}^Q(\Omega_m) = -\frac{3T}{8} \sum_{|\omega_m| < \omega_0} \frac{\Delta_{k_\pi}^Q(\Omega_{m'})}{|\Omega_{m'}|} \int_0^\infty \frac{dz}{\sqrt{z^2 + |1 - \Omega_{m'}/\Omega_m|}} \frac{1}{z^2 + 9/64}, \quad (17)$$

$$\Delta_{k_\pi}^Q(\Omega_m) = -\frac{3T}{8} \sum_{|\omega_m| < \omega_0} \frac{\Delta_{k_0}^Q(\Omega_{m'})}{|\Omega_{m'}|} \int_0^\infty \frac{dz}{\sqrt{z^2 + |1 - \Omega_{m'}/\Omega_m|}} \frac{1}{\left(\sqrt{z^2 + |1 - \Omega_{m'}/\Omega_m|} + 3/8\right)^2}, \quad (18)$$

We search for the solution in the form  $\Delta_{k_0}^Q, \Delta_{k_\pi}^Q \sim |\Omega_m|^{-\alpha}$ . One can easily verify that convergence of integrals requires  $0 < \alpha < 0.5$ . Substituting this trial solution into (18) we find after simple algebra a self-consistency condition

$$bF(\alpha)G(\alpha) = 1, \quad (19)$$

where  $b = 9/64$  is the universal dimensionless coupling constant for our quantum-critical problem, and

$$F(\alpha) = \frac{1}{2\pi} \int_{-\infty}^{\infty} \frac{d\omega}{|\omega|^{1+\alpha}} \int_0^\infty \frac{dz}{\sqrt{z^2 + |1 - 1/\omega|}} \frac{1}{\left(\sqrt{z^2 + |1 - 1/\omega|} + 3/8\right)^2}$$

$$G(\alpha) = \frac{1}{2\pi} \int_{-\infty}^{\infty} \frac{d\omega}{|\omega|^{1+\alpha}} \int_0^\infty \frac{dz}{\sqrt{z^2 + |1 - 1/\omega|}} \frac{1}{z^2 + 9/64}, \quad (20)$$

We solved Eq. (19) for  $\alpha$  and found that the solution is a complex number:  $\alpha = 0.288 \pm 0.185i$ . This implies that the power-law solution has a phase factor, which can be adjusted to fit the boundary condition at the upper end of the power-law behavior. The boundary condition at the lower end can then be met at some  $T_{CDW} \sim \omega_0$ . At this temperature, the set of linearized equations (18) for  $\Delta_{k_0}^Q(\Omega_m)$  and  $\Delta_{k_\pi}^Q(\Omega_m)$  has a solution, i.e., the system does become unstable towards a CDW order. We didn't attempt to calculate  $T_{CDW}$  with the prefactor as it would require a more precise analysis with the soft rather than hard cutoff at frequencies of order  $\omega_0$ . We did, however, compared the set of equations for  $T_{CDW}$  with the equation for  $T_c$  in the spin-fluctuation approach (see Sec.IX A below). We did find that both  $T_c$  and  $T_{CDW}$  are of order  $\omega_0$ , and the numerical prefactor is a bit larger for  $T_c$ . To obtain the ratio  $T_c/T_{CDW}$ , one needs to solve full integral gap equations in momentum and frequency, which we didn't do. We recall that our point is that  $T^*$  is larger than  $T_{CDW}$  and well can be larger than  $T_c$  despite that  $T_{CDW} \leq T_c$ .

### C. The behavior of $T_{CDW}$ at a finite magnetic correlation length $\xi$

The key point for the analysis of how  $T_{CDW}(\xi)$  evolves when hole doping increases and magnetic correlation length decreases, is that a finite  $\xi$  by itself introduces the lower energy cut-off for the power-law behavior. As a result, the energy scale, down to which the power-law behavior  $\Omega_m^{-\alpha}$  holds, gets larger than  $T$  and, roughly, becomes  $(T^2 + \bar{g}^2/\lambda^4)^{1/2}$ , where  $\lambda \sim \bar{g}\xi/v_F$ . Accordingly,  $T_{CDW}(\xi)$  decreases, as  $T_{CDW}(\xi) \sim T_{CDW}(\xi = \infty) (1 - a/\lambda^2)$ , where  $a = O(1)$ . At some critical  $\lambda = O(1)$ , i.e., critical  $\xi_{cr}^{-1} \sim k_F(E_F/\bar{g}) \gg k_F$ ,  $T_{CDW}$  vanishes. The vanishing of  $T_{CDW}(\xi_{cr})$  sets up a charge QCP at some distance away from a magnetic QCP (see Fig. 3 in the main text).

The behavior of  $T_{CDW}(\xi)$  is different from that of superconducting  $T_c(\xi)$ . The latter does not vanish at a finite  $\xi$  and just interpolates between quantum-critical form  $T_c \sim \omega_0$  at large  $\xi$  and BCS form  $T_c \propto \omega_0 e^{-1/\lambda}$  at smaller  $\xi$ , when  $\lambda$  becomes a small parameter. We discuss the behavior of superconducting  $T_c$  in more detail in Sec.IX below.

## VI. STRIPE VS CHECKERBOARD ORDER: GINZBURG-LANDAU ANALYSIS

In this part we present the details of the derivation of Eq. (2) in the main text.

### A. The effective action

Consider first the ordering along  $y$  direction, between regions 1-2 and 3-4. The 4-fermion interaction, which provides the ‘‘pairing glue’’, is  $H' = 3\bar{g}\chi c_{k_0-Q}^\dagger c_{k_0+Q} c_{k_\pi+Q}^\dagger c_{k_\pi-Q} + h.c.$ . We define  $\bar{\chi} = 3\bar{g}\chi$ ,  $\rho_{k_0}^Q = c_{k_0+Q}^\dagger c_{k_0-Q}$ , and  $\rho_{k_\pi}^Q = c_{k_\pi+Q}^\dagger c_{k_\pi-Q}$ , and rewrite the 4-fermion interaction as,

$$H' = \bar{\chi} \left( \bar{\rho}_{k_0}^Q \rho_{k_\pi}^Q + \bar{\rho}_{k_\pi}^Q \rho_{k_0}^Q \right) = \frac{\bar{\chi}}{2} \left( \bar{\rho}_{k_0}^Q + \bar{\rho}_{k_\pi}^Q \right) \left( \rho_{k_0}^Q + \rho_{k_\pi}^Q \right) - \frac{\bar{\chi}}{2} \left( \bar{\rho}_{k_0}^Q - \bar{\rho}_{k_\pi}^Q \right) \left( \rho_{k_0}^Q - \rho_{k_\pi}^Q \right). \quad (21)$$

The conventional way to obtain the action in terms of collective variables is to perform Hubbard-Stratonovich transformation<sup>6,7</sup>,

$$\begin{aligned} & \exp[-\bar{\chi} \left( \bar{\rho}_{k_0}^Q \rho_{k_\pi}^Q + \bar{\rho}_{k_\pi}^Q \rho_{k_0}^Q \right)] = \exp \left[ -\frac{\bar{\chi}}{2} \left( \bar{\rho}_{k_0}^Q + \bar{\rho}_{k_\pi}^Q \right) \left( \rho_{k_0}^Q + \rho_{k_\pi}^Q \right) \right] \times \exp \left[ \frac{\bar{\chi}}{2} \left( \bar{\rho}_{k_0}^Q - \bar{\rho}_{k_\pi}^Q \right) \left( \rho_{k_0}^Q - \rho_{k_\pi}^Q \right) \right] \\ & = \int d\bar{\Delta}_{k_0}^Q d\bar{\Delta}_{k_\pi}^Q d\Delta_{k_0}^Q d\Delta_{k_\pi}^Q \exp \left[ \frac{1}{2\bar{\chi}} (\bar{\Delta}_{k_0}^Q + \bar{\Delta}_{k_\pi}^Q) (\Delta_{k_0}^Q + \Delta_{k_\pi}^Q) + \frac{1}{2} (\bar{\Delta}_{k_0}^Q + \bar{\Delta}_{k_\pi}^Q) (\rho_{k_0}^Q + \rho_{k_\pi}^Q) + \frac{1}{2} (\bar{\rho}_{k_0}^Q + \bar{\rho}_{k_\pi}^Q) (\Delta_{k_0}^Q + \Delta_{k_\pi}^Q) \right] \\ & \quad \times \exp \left[ -\frac{1}{2\bar{\chi}} (\bar{\Delta}_{k_0}^Q - \bar{\Delta}_{k_\pi}^Q) (\Delta_{k_0}^Q - \Delta_{k_\pi}^Q) + \frac{1}{2} (\bar{\Delta}_{k_0}^Q - \bar{\Delta}_{k_\pi}^Q) (\rho_{k_0}^Q - \rho_{k_\pi}^Q) + \frac{1}{2} (\bar{\rho}_{k_0}^Q - \bar{\rho}_{k_\pi}^Q) (\Delta_{k_0}^Q - \Delta_{k_\pi}^Q) \right] \\ & = \int d\bar{\Delta}_{k_0}^Q d\bar{\Delta}_{k_\pi}^Q d\Delta_{k_0}^Q d\Delta_{k_\pi}^Q \exp \left[ \frac{1}{\bar{\chi}} (\bar{\Delta}_{k_0}^Q \Delta_{k_\pi}^Q + \bar{\Delta}_{k_\pi}^Q \Delta_{k_0}^Q) + \bar{\Delta}_{k_0}^Q \rho_{k_\pi}^Q + \bar{\Delta}_{k_\pi}^Q \rho_{k_0}^Q + \bar{\rho}_{k_\pi}^Q \Delta_{k_0}^Q + \bar{\rho}_{k_0}^Q \Delta_{k_\pi}^Q \right]. \quad (22) \end{aligned}$$

Integrating out the fermionic degrees of freedom and expanding the result to quadratic order in  $\Delta$  we obtain the effective action

$$S_{\text{eff}}^{(2)} = -\frac{1}{\bar{\chi}} \left( \bar{\Delta}_{k_0}^Q \Delta_{k_\pi}^Q + \bar{\Delta}_{k_\pi}^Q \Delta_{k_0}^Q \right) + A_1 \left| \Delta_{k_0}^Q \right|^2 + A_2 \left| \Delta_{k_\pi}^Q \right|^2, \quad (23)$$

where  $A_1$  and  $A_2$  are bilinear combinations of fermionic propagators shown graphically in Fig. 7. The extremal

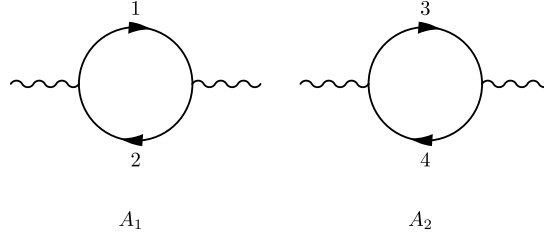


FIG. 7: The diagrams for the coefficients  $A_1$  and  $A_2$  in the effective action, Eq. (23).

condition on the effective action yields

$$\begin{aligned}\Delta_{k_\pi}^Q &= \bar{\chi} A_1 \Delta_{k_0}^Q \\ \Delta_{k_0}^Q &= \bar{\chi} A_2 \Delta_{k_\pi}^Q.\end{aligned}\quad (24)$$

Because the gap functions and the interaction are momentum and frequency dependent, i.e.,  $\bar{\chi} = \bar{\chi}(k, \omega_m; k', \omega'_m)$  and  $\Delta_k^Q = \Delta_k^Q(k, \omega_m)$ , the products above should be understood as matrix products. One can easily make sure that Eqs. (24) are the same as the linearized gap equations, Eqs. (8) and (9).

For simplicity, we will treat  $\Delta_{k_0}^Q$  and  $\Delta_{k_\pi}^Q$  as frequency independent, i.e., treat (24) as algebraic equations. Evaluating the diagrams in Fig. 7 we find that  $A_1 < A_2 < 0$ , hence  $\Delta_{k_0}^Q$  and  $\Delta_{k_\pi}^Q$  differ in sign. The critical temperature  $T_{\text{CDW}}$  is given by the condition  $\bar{\chi}\sqrt{A_1 A_2} = 1$  and the solution satisfies  $\mu = -\Delta_{k_\pi}^Q / \Delta_{k_0}^Q = \sqrt{A_2 / A_1} > 1$ . This is fully consistent with the full solution of the linearized gap equations in the previous Section. Defining  $\Delta_y \equiv \Delta_{k_0}^Q$  and plugging in the results above, one finds

$$\mathcal{S}_{\text{eff}}^{(2)} = 2\sqrt{\frac{A_1}{A_2}} \left( \frac{1}{\bar{\chi}} - \sqrt{A_1 A_2} \right) |\Delta_y|^2 = \alpha |\Delta_y|^2 \quad (25)$$

where  $\alpha = a(T - T_{\text{CDW}})$  and  $a > 0$ .

The same analysis can be performed for the order along x direction. The prefactors for  $|\Delta_y|^2$  and  $|\Delta_x|^2$  are indeed the same by symmetry, and the full action to order  $\Delta^2$  is

$$\mathcal{S}_{\text{eff}}^{(2)} = \alpha (|\Delta_x|^2 + |\Delta_y|^2) \quad (26)$$

Next we move to the quartic terms. We keep the condition  $\Delta_{k_\pi}^Q = \mu \Delta_{k_0}^Q$  and expand the effective action to order  $\Delta^4$ . We obtain

$$\mathcal{S}_{\text{eff}} = \alpha (|\Delta_x|^2 + |\Delta_y|^2) + \beta_1 (|\Delta_x|^4 + |\Delta_y|^4) + 2\beta_2 |\Delta_x|^2 |\Delta_y|^2 \quad (27)$$

where

$$\begin{aligned}\beta_1 &= -2(I_1 + \mu^4 I_2) \\ \beta_2 &= -2\mu^2(2I_3 + I_4),\end{aligned}\quad (28)$$

and  $I_i$  are the convolutions of four fermionic propagators

$$\begin{aligned}I_1 &\equiv -\frac{1}{2} \int G_1^2 G_2^2 \\ I_2 &\equiv -\frac{1}{2} \int G_1^2 G_5^2 \\ I_3 &\equiv -\int G_1 G_5^2 G_6 \\ I_4 &\equiv -\int G_1 G_2 G_5 G_6\end{aligned}\quad (29)$$

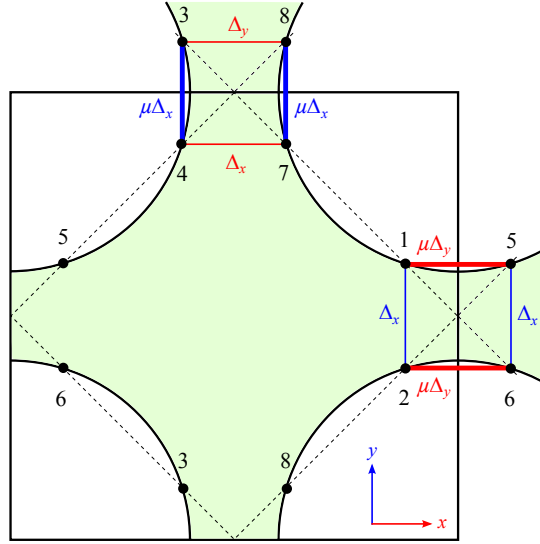


FIG. 8: The two order parameters responsible for stripe or checkerboard order.

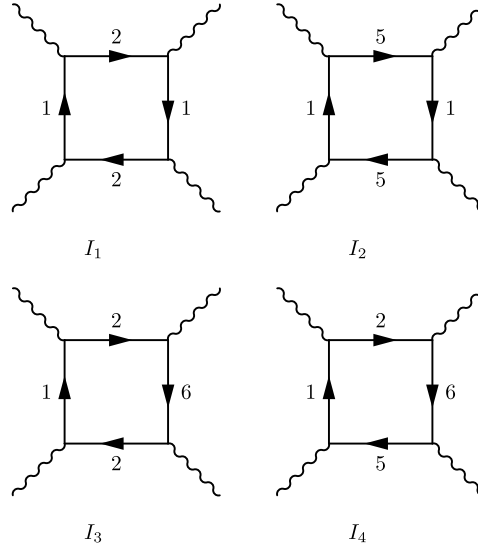


FIG. 9: The diagrammatic representation of the prefactors for the quartic terms in the effective action.

We show  $I_i$  graphically in Fig. 9. The overall minus sign in every line is due to the presence of a fermionic loop. The abbreviations for the Green's function as  $G_1 \equiv G(\omega_m, \mathbf{k}_1 + (k_x, k_y))$ , etc, and the integrals are performed over running frequency  $\omega_m$  and momenta  $k_x$  and  $k_y$ .

Quite generally, whether an effective action with two order parameters, given by Eq. (27), gives rise to a checkerboard order, in which both  $\Delta_x$  and  $\Delta_y$  develop simultaneously, or to a stripe order, in which only one order develops, is determined by comparison of the coefficients  $\beta_1$  and  $\beta_2$ . When  $\beta_1 > |\beta_2|$ , a checkerboard order develops, and for  $\beta_1 < |\beta_2|$  a stripe order develops. This is true when  $\beta_1 > 0$ , otherwise the transition is first order.

### B. Evaluation of the integrals $I_1$ $I_2$ $I_3$ and $I_4$

For  $I_1$  we explicitly obtain

$$I_1 = -\frac{T}{2} \sum_m \int_{-\Lambda}^{\Lambda} \frac{dk_x dk_y}{(2\pi)^2} \left[ \frac{1}{i\omega_m - (v_x k_x + v_y k_y)} \right]^2 \left[ \frac{1}{i\omega_m - (v_x k_x - v_y k_y)} \right]^2 \quad (30)$$

We keep the upper cutoff  $\Lambda$  in the momentum integrals. i.e., integrate over a finite momentum range around hot spots. We will take the limit  $v_x \ll v_y$ , but  $v_x \Lambda \gg T$ . Introducing the new parameters,

$$x = v_x k_x, \quad y = v_y k_y, \quad \Lambda_x = v_x \Lambda, \quad \Lambda_y = v_y \Lambda \gg \Lambda_x. \quad (31)$$

we re-write  $I_1$  as

$$I_1 = -\frac{T}{8\pi^2 v_x v_y} \sum_m \int_{-\Lambda_x}^{\Lambda_x} dx \int_{-\Lambda_y}^{\Lambda_y} dy \left( \frac{1}{y+x-i\omega_m} \right)^2 \left( \frac{1}{y-x+i\omega_m} \right)^2. \quad (32)$$

We separate the  $y$ -integral  $\int_{-\Lambda_y}^{\Lambda_y} dy$  into  $I_1 = \int_{-\infty}^{\infty} dy - \int_{|y|>\Lambda_y} dy \equiv I_{1a} - I_{1b}$ . For  $I_{1a}$  we obtain

$$\begin{aligned} I_{1a} &= -\frac{T}{8\pi^2 v_x v_y} \sum_m \int_{-\Lambda_x}^{\Lambda_x} dx \int_{-\infty}^{\infty} dy \left( \frac{1}{y+x-i\omega_m} \right)^2 \left( \frac{1}{y-x+i\omega_m} \right)^2 \\ &= -\frac{iT}{16\pi v_x v_y} \sum_m \operatorname{sgn}(\omega_m) \int_{-\Lambda_x}^{\Lambda_x} dx \left( \frac{1}{x-i\omega_m} \right)^3 \\ &= -\frac{iT}{16\pi v_x v_y} \sum_m \int_{-\Lambda_x}^{\Lambda_x} dx \left( \frac{1}{x-i|\omega_m|} \right)^3 \\ &= -\frac{iT}{32\pi v_x v_y} \sum_m \left[ \left( \frac{1}{|\omega_m|+i\Lambda_x} \right)^2 - \left( \frac{1}{|\omega_m|-i\Lambda_x} \right)^2 \right] \\ &\approx -\frac{i}{64\pi^2 v_x v_y} \int d\omega \left[ \left( \frac{1}{|\omega|+i\Lambda_x} \right)^2 - \left( \frac{1}{|\omega|-i\Lambda_x} \right)^2 \right] \\ &= -\frac{1}{16\pi^2 v_x v_y} \frac{1}{\Lambda_x}. \end{aligned} \quad (33)$$

In the second to last line we used  $\Lambda_x \gg T$ . Note that the original integrand is singular in the infra-red, so it is important to keep the temperature *finite* as a regulator of the singularity and set  $T \rightarrow 0$  only at the very end of calculations. We will use the same procedure for the other integrals.

The contribution to  $I_1$  from  $|y| > \Lambda_y$  is

$$\begin{aligned} I_{1b} &= -\frac{T}{8\pi^2 v_x v_y} \sum_m \int_{-\Lambda_x}^{\Lambda_x} dx \int_{|y|>\Lambda_y} dy \left( \frac{1}{y+x-i\omega_m} \right)^2 \left( \frac{1}{y-x+i\omega_m} \right)^2 \\ &= -\frac{T\Lambda_x}{2\pi^2 v_x v_y} \sum_m \int_{\Lambda_y}^{\infty} \frac{1}{(y^2 + \omega_m^2)^2} \\ &= -\frac{1}{16\pi^2 v_x v_y} \frac{\Lambda_x}{\Lambda_y^2}. \end{aligned} \quad (34)$$

In the first line we used the fact that  $\Lambda_y \gg \Lambda_x$ . As we see, both contributions are small in  $1/\Lambda$ . The full result for  $I_1$  is

$$I_1 = -\frac{1}{16\pi^2 v_x v_y} \left( \frac{1}{\Lambda_x} - \frac{\Lambda_x}{\Lambda_y^2} \right) \approx -\frac{1}{16\pi^2 v_x^2 v_y} \frac{1}{\Lambda} \quad (35)$$

For  $I_2$  we have, in terms of new parameters introduced in Eq. 31,

$$I_2 = -\frac{T}{8\pi^2 v_x v_y} \sum_m \int_{-\Lambda_x}^{\Lambda_x} dx \int_{-\Lambda_y}^{\Lambda_y} dy \left( \frac{1}{x+y-i\omega_m} \right)^2 \left( \frac{1}{x-y+i\omega_m} \right)^2. \quad (36)$$

We again separate the integral over  $y$  as  $I_2 = \int_{-\infty}^{\infty} dy - \int_{|y|>\Lambda_y} dy \equiv I_{2a} - I_{2b}$ . This time, the integral over  $y$  from



$-\infty$  to  $\infty$  vanishes because the poles are all located in the same half plane. The integral  $I_{2b}$  also vanishes:

$$\begin{aligned}
I_{2b} &= -\frac{T}{8\pi^2 v_x v_y} \sum_m \int_{-\Lambda_x}^{\Lambda_x} dx \int_{|y|>\Lambda_y} dy \left( \frac{1}{x+y-i\omega_m} \right)^2 \left( \frac{1}{x-y+i\omega_m} \right)^2 \\
&= -\frac{T\Lambda_x}{4\pi^2 v_x v_y} \sum_m \int_{\Lambda_y}^{\infty} \left[ \left( \frac{1}{y-i\omega_m} \right)^4 + \left( \frac{1}{y+i\omega_m} \right)^4 \right] \\
&\approx -\frac{\Lambda_x}{8\pi^3 v_x v_y} \int d\omega \int_{\Lambda_y}^{\infty} \left[ \left( \frac{1}{y-i\omega} \right)^4 + \left( \frac{1}{y+i\omega} \right)^4 \right] \\
&= 0.
\end{aligned} \tag{37}$$

As a result,

$$I_2 = 0. \tag{38}$$

Now we turn to  $I_3$ . We explicitly write it down as

$$I_3 = \frac{T}{4\pi^2 v_x v_y} \sum_m \int_{-\Lambda_x}^{\Lambda_x} dx \int_{-\Lambda_y}^{\Lambda_y} dy \left( \frac{1}{x+y-i\omega_m} \right)^2 \frac{1}{(x-y)^2 + \omega_m^2}. \tag{39}$$

As before, we write  $I_3 = \int_{-\infty}^{\infty} dy - \int_{|y|>\Lambda_y} dy \equiv I_{3a} - I_{3b}$ . We evaluate  $I_{3a}$  by extending the integral over  $y$  onto the half plane where the integrand contains a single pole

$$\begin{aligned}
I_{3a} &= \frac{T}{4\pi^2 v_x v_y} \sum_m \int_{-\Lambda_x}^{\Lambda_x} dx \int_{-\infty}^{\infty} dy \left( \frac{1}{x+y-i\omega_m} \right)^2 \frac{1}{(x-y)^2 + \omega_m^2} \\
&= \frac{T}{16\pi v_x v_y} \sum_m \operatorname{sgn}(\omega_m) \int_{-\Lambda_x}^{\Lambda_x} dx \left( \frac{1}{x-i\omega_m} \right)^2 \frac{1}{\omega_m} \\
&= -\frac{T}{16\pi v_x v_y} \sum_m \operatorname{sgn}(\omega_m) \frac{2\Lambda_x}{\Lambda_x^2 + \omega_m^2} \frac{1}{\omega_m} \\
&\approx -\frac{1}{16\pi^2 v_x v_y} \frac{1}{\Lambda_x} \log \frac{\omega_0}{T}.
\end{aligned} \tag{40}$$

We see that  $I_{3a}$  is logarithmically singular at  $T \rightarrow 0$ . The other part,  $I_{3b}$ , is regular at  $T \rightarrow 0$ , i.e., is much smaller. Therefore,

$$I_3 \approx -\frac{1}{16\pi^2 v_x^2 v_y} \frac{1}{\Lambda} \log \frac{\omega_0}{T}. \tag{41}$$

Finally, for  $I_4$  we have

$$I_4 = -\frac{T}{4\pi^2 v_x v_y} \sum_m \int_{-\Lambda_x}^{\Lambda_x} dx \int_{-\Lambda_y}^{\Lambda_y} dy \frac{1}{(x+y)^2 + \omega_m^2} \frac{1}{(x-y)^2 + \omega_m^2}. \tag{42}$$

The most straightforward way to evaluate this integral is to first extend both  $x$ - and  $y$ -integrations to infinite limits and then check how the results change when we restore finite limits of integration. To evaluate the integral in infinite limits, we introduce new variables  $a = x + y$  and  $b = x - y$ , in terms of which

$$\begin{aligned}
I_4 &= -\frac{T}{8\pi^2 v_x v_y} \sum_m \int_{-\infty}^{\infty} da \int_{-\infty}^{\infty} db \frac{1}{a^2 + \omega_m^2} \frac{1}{b^2 + \omega_m^2} \\
&= -\frac{1}{8v_x v_y} T \sum_{\omega_m} \frac{1}{\omega_m^2} \\
&= -\frac{1}{32v_x v_y} \frac{1}{T}.
\end{aligned} \tag{43}$$

We see that  $I_4$  diverges as  $1/T$ . The divergence obviously comes from momenta much smaller than  $\Lambda$ , hence it does not depend on whether the limits of momentum integration are infinite or finite. Finite limits only give rise to small corrections to (43) of order  $1/\Lambda$ .

Combining the results for  $I_i$ , we find that the prefactors  $\beta_1$  and  $\beta_2$  in Eq. (31) are given by

$$\begin{aligned}\beta_1 &= -2(I_1 + \mu^4 I_2) = \frac{1}{8\pi v_x^2 v_y} \frac{1}{\Lambda}, \\ \beta_2 &= -2\mu^2(2I_3 + I_4) = \frac{2\mu^2}{8\pi v_x^2 v_y} \left( \frac{1}{\Lambda} \log \frac{\omega_0}{T} + \frac{\pi}{4T} \right).\end{aligned}\quad (44)$$

Because  $\mu > 1$ , we obviously have  $|\beta_2| \gg \beta_1$ , i.e., the system overwhelmingly chooses stripe order in which only  $\Delta_x$  or  $\Delta_y$  emerges. Such an order spontaneously breaks  $C_4$  lattice rotational symmetry.

A remark is in order. In the above analysis we assumed that  $\Delta_k^Q = \Delta_{-k}^Q$ , i.e., that the CDW order parameter is even in  $k$ . We will see in the next section that in reality both even and odd components of  $\Delta_k^Q$  develop below  $T_{\text{CDW}}$ . Still, the reasoning for the stripe order remains valid. The argument is the following: the inclusion of both even and odd components of  $\Delta_k^Q$  only changes the phase of  $\beta_2$ , but not its magnitude, and, as long as  $|\beta_2| > \beta_1$ , the system still unambiguously prefers a stripe order.

To see this explicitly, assume that  $\Delta_x$  and  $\Delta_y$  are complex. Re-deriving the effective action for complex  $\Delta_{x,y}$  we obtain

$$\mathcal{S}_{\text{eff}} = \alpha(|\Delta_x|^2 + |\Delta_y|^2) + \beta_1(|\Delta_x|^4 + |\Delta_y|^4) + 8\mu^2 I_3 |\Delta_x|^2 |\Delta_y|^2 + 2\mu^2 I_4 [\Delta_x^2 \Delta_y^2 + (\Delta_x^2)^* (\Delta_y^2)^*] \quad (45)$$

One can easily see that the action is minimized when the relative phase between  $\Delta_x$  and  $\Delta_y$  is  $\pm\pi/2$ . For these values of the relative phase we have

$$\mathcal{S}_{\text{eff}} = \alpha(|\Delta_x|^2 + |\Delta_y|^2) + \beta_1(|\Delta_x|^4 + |\Delta_y|^4) - \beta'_2 |\Delta_x^2| |\Delta_y^2|, \quad (46)$$

where  $\beta'_2 \equiv -2\mu^2(2I_3 - I_4)$ . Comparing with Eq. (27) we see that the only change is the sign in front of  $I_4$ . Substituting the results for  $I_i$ , we find  $|\beta'_2| > \beta_1$ , i.e., even in this situation the system still develops a stripe CDW order.

## VII. DENSITY AND CURRENT COMPONENT OF $\Delta_k^Q$

### A. The effective action and mean-field analysis

Like we said in the main text,  $\Delta_k^Q$  generally has both even and odd in  $k$  components, and the equations for the two are identical if we restrict the “gap equation” to near vicinities of hot spots and approximate  $\Delta_k^Q$  by its value at  $k$  in between the neighboring hot spots. To derive the effective action, we choose the CDW order along  $y$  direction ( $k \approx k_0$  and  $k \approx k_\pi$ ), use  $\Delta_{k_\pi}^Q = -\mu \Delta_{k_0}^Q$ , and split  $\Delta_{k_0}^Q$  into a part even in  $k_0$  and a part odd in  $k_0$

$$\Delta_k^Q = \Delta_1^Q + \Delta_2^Q \text{sgn}(k). \quad (47)$$

Using again Hubbard-Stratonovich transformation and following the same steps as in the previous Section, we obtain the effective action in terms of  $\Delta_1$  and  $\Delta_2$  in the form

$$\begin{aligned}\mathcal{S}_{\text{eff}} &= \alpha(|\Delta_1^Q|^2 + |\Delta_2^Q|^2) + \frac{\beta_1}{2} \left( |\Delta_1^Q + \Delta_2^Q|^4 + |\Delta_1^Q - \Delta_2^Q|^4 \right) \\ &= \alpha(|\Delta_1^Q|^2 + |\Delta_2^Q|^2) + \beta_1(|\Delta_1^Q|^2 + |\Delta_2^Q|^2)^2 + \beta_1((\Delta_1^Q)^* \Delta_2^Q + \Delta_1^Q (\Delta_2^Q)^*)^2,\end{aligned}\quad (48)$$

where  $\beta_1 = I_1 + \mu^4 I_2$ . This is the Eq. (3) in the main text.

Without loss of generality, we can set  $\Delta_1$  to be real, and we keep  $\Delta_2$  as a complex field. At the mean-field level, the minimization of the effective action immediately shows that the phase difference between  $\Delta_2^Q$  and  $\Delta_1^Q$  should be  $\pm\pi/2$ , i.e., when  $\Delta_1$  is real,  $\Delta_2$  should be imaginary. The generic condition  $(\Delta_k^Q)^* = \Delta_k^{-Q}$  then imposes the constraint that  $\Delta_1$  must be even in  $Q$  and  $\Delta_2$  must be odd in  $Q$ , i.e.,

$$\Delta_k^Q = \Delta_1^Q \pm i|\Delta_2^Q| \text{sgn}(k) \text{sgn}(Q). \quad (49)$$

This is the Eq. (4) in the main text.

Converting to real space, we find that the first term corresponds to an incommensurate modulation on local charge density in  $y$  direction,

$$\begin{aligned}\delta\rho(r) &= \langle c^\dagger(r)c(r) \rangle \\ &= \sum_k \langle c^\dagger(k+Q_y)c(k-Q_y) \rangle e^{i(k+Q_y)r} e^{-i(k-Q_y)r} + h.c. \\ &\propto \Delta_1^Q \cos 2Qr_y,\end{aligned}\tag{50}$$

and the second term corresponds to an incommensurate bond current, which flows along  $x$  direction and has incommensurate modulation in  $y$  direction:

$$\begin{aligned}j_x(r) &= \text{Re} [i \langle c^\dagger(r-a_x/2)c(r+a_x/2) \rangle] \\ &= \text{Re} \left[ i \sum_k \langle c^\dagger(k+Q_y)c(k-Q_y) \rangle e^{i(k+Q_y)(r-a_x/2)} e^{-i(k-Q_y)(r+a_x/2)} + (Q_y \rightarrow -Q_y) \right] \\ &= \text{Re} \left[ i \sum_k (\Delta_k^Q e^{2iQr_y} + \Delta_k^{-Q} e^{-2iQr_y}) e^{-ik} \right] \\ &= 2\text{Re} \left[ i \Delta_1^Q \cos(2Qr_y) \sum_k e^{-ik} - i |\Delta_2^Q| \sin(2Qr_y) \sum_k \text{sgn}(k) e^{-ik} \right] \\ &\propto |\Delta_2^Q| \sin 2Qr_y \sin k_0 = |\Delta_2^Q| \sin 2Qr_y \sin Q,\end{aligned}\tag{51}$$

where  $a_x$  is the unit lattice vector along  $x$  direction.

## B. Preemptive loop-current order

Beyond mean-field approximation,  $\Delta_1$  and  $\Delta_2$  have to be considered as fluctuating fields. In this subsection we present the details of the analysis of a preemptive transition above  $T_{\text{CDW}}$ , at which a composite order  $\langle \Delta_1^Q \Delta_2^{-Q} \rangle$  emerges, while  $\langle \Delta_1^Q \rangle = \langle \Delta_2^Q \rangle = 0$ .

To see this, we re-write the effective action (48) as

$$\begin{aligned}\mathcal{S}_{\text{eff}} &= \alpha(|\Delta_1^Q|^2 + |\Delta_2^Q|^2) + \beta_1(|\Delta_1^Q|^4 + |\Delta_2^Q|^4) \\ &\quad + \beta_1(\Delta_1^Q(\Delta_2^Q)^*)(\Delta_1^Q(\Delta_2^Q)^*) + \beta_1((\Delta_1^Q)^*\Delta_2^Q)((\Delta_1^Q)^*\Delta_2^Q) + 4\beta_1(\Delta_1^Q(\Delta_2^Q)^*)(\Delta_2^Q(\Delta_1^Q)^*).\end{aligned}\tag{52}$$

One way to see that a preemptive transition is possible is to follow the same strategy as in the analysis of a spin-current order in anisotropic triangular antiferromagnets<sup>8</sup>, i.e., introduce a “two-particle” collective variable  $\bar{\Upsilon} = \Delta_1^Q \Delta_2^{-Q} = \Delta_1^Q(\Delta_2^Q)^*$  and solve for the emergence of a two-particle bound state instability in the same way as it is done for superconductivity. The ladder equation for  $\bar{\Upsilon}$  is presented in Fig. 10 There are two terms in the r.h.s. of this graphic equation – the first contains a “direct”  $\bar{\Upsilon}\bar{\Upsilon}$  interaction from the first term in the second line of (52), and the second one contains the interaction between  $\bar{\Upsilon}$  and  $\bar{\Upsilon}^*$ . Both interactions are repulsive, hence no solution is possible if  $\bar{\Upsilon}$  is real. However, if we search for a solution with a complex  $\bar{\Upsilon}$ , we obtain for infinitesimally small  $\bar{\Upsilon}$

$$\bar{\Upsilon} = -\beta_1 P (\bar{\Upsilon} + 4\bar{\Upsilon}^*)\tag{53}$$

where  $P > 0$  stand for convolution of the propagators of  $\Delta_1^Q$  and  $\Delta_2^Q$  fields. The only information about  $P$  relevant to us at this stage is that it diverges at  $T_{\text{CDW}}$  when both propagators become massless. Hence, if Eq. (53) has a non-trivial solution, the corresponding  $T$  is larger than  $T_{\text{CDW}}$ . A simple analysis of Eq. (53) shows that the solution does exist if we set  $\bar{\Upsilon}$  to be purely imaginary,  $\bar{\Upsilon} = i\Upsilon$ , because then the combination  $\bar{\Upsilon} + 4\bar{\Upsilon}^*$  becomes equal to  $-3\bar{\Upsilon}$ , and the minus sign compensates the overall minus sign in the r.h.s. of (53). We emphasize that this is possible because the prefactor for  $\bar{\Upsilon}\bar{\Upsilon}^*$  interaction term (the last term in (52)) is 4 times larger than the direct  $\bar{\Upsilon}\bar{\Upsilon}$  interaction term. That  $\bar{\Upsilon}$  is purely imaginary is entirely consistent with the fact that in mean-field approximation  $\Delta_1^Q$  is real and  $\Delta_2^Q$  is imaginary, hence in below  $T_{\text{CDW}}$ ,  $\bar{\Upsilon} = \Delta_1^Q \Delta_2^{-Q}$  is also purely imaginary.

Another way to see the emergence of a preemptive transition is to follow the same strategy as in the analysis of spin-nematic instability in Fe-pnictides<sup>6</sup>, introduce  $\Upsilon$  as a real field, conjugated to an anti-symmetrized combination

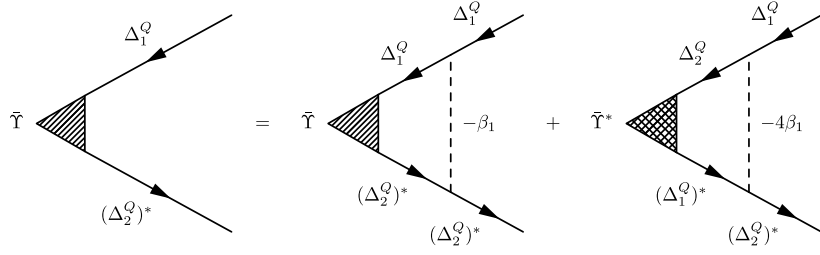


FIG. 10: Ladder equation for  $\tilde{\Upsilon} = \Delta_1^Q (\Delta_2^Q)^*$ . Of the two terms in the r.h.s., one contains  $\tilde{\Upsilon}$ , another  $\tilde{\Upsilon}^*$ . For imaginary  $\tilde{\Upsilon}$ , there is a sign change between these two terms.

$i(\Delta_1^Q \Delta_2^{-Q} - \Delta_1^{-Q} \Delta_2^Q) \equiv i(\Delta_1^Q (\Delta_2^Q)^* - (\Delta_1^Q)^* \Delta_2^Q)$  and analyze the effective action  $S(\Upsilon)$ . If this action acquires a minimum at a finite  $\Upsilon$  below some  $T > T_{\text{CDW}}$ , the system develops a non-zero imaginary order  $\langle \Delta_1^Q \Delta_2^{-Q} \rangle = \pm i|\Upsilon|$ .

To obtain the action in terms of  $\Upsilon$ , we rewrite Eq. (48) as

$$\mathcal{S}_{\text{eff}} = \alpha(|\Delta_1^Q|^2 + |\Delta_2^Q|^2) + 2\beta_1(|\Delta_1^Q|^2 + |\Delta_2^Q|^2)^2 + \beta_1((\Delta_1^Q)^* \Delta_2^Q - \Delta_1^Q (\Delta_2^Q)^*)^2 - \beta_1(|\Delta_1^Q|^2 - |\Delta_2^Q|^2)^2, \quad (54)$$

and introduce, via Hubbard-Stratonovich transformation, three collective fields:  $\tilde{\Phi}$ , conjugated to  $i(|\Delta_1^Q|^2 + |\Delta_2^Q|^2)$ ,  $\Psi$ , conjugated to  $|\Delta_1^Q|^2 - |\Delta_2^Q|^2$ , and  $\Upsilon$ , conjugated to  $i(\Delta_1^Q (\Delta_2^Q)^* - (\Delta_1^Q)^* \Delta_2^Q)$ , as

$$\begin{aligned} \exp[-2\beta_1(|\Delta_1^Q|^2 + |\Delta_2^Q|^2)^2] &= \int \frac{d\tilde{\Phi}}{\sqrt{8\pi\beta_1}} \exp\left(\frac{-\tilde{\Phi}^2}{8\beta_1}\right) \exp\left[i\tilde{\Phi}(|\Delta_1^Q|^2 + |\Delta_2^Q|^2)\right] \\ \exp[\beta_1(|\Delta_1^Q|^2 - |\Delta_2^Q|^2)^2] &= \int \frac{d\Psi}{\sqrt{4\pi\beta_1}} \exp\left(-\frac{\Psi^2}{4\beta_1}\right) \exp\left[\Psi(|\Delta_1^Q|^2 - |\Delta_2^Q|^2)\right] \\ \exp[-\beta_1(\Delta_1^Q (\Delta_2^Q)^* - (\Delta_1^Q)^* \Delta_2^Q)^2] &= \int \frac{d\Upsilon}{\sqrt{4\pi\beta_1}} \exp\left(-\frac{\Upsilon^2}{4\beta_1}\right) \exp\left[i\Upsilon(\Delta_1^Q (\Delta_2^Q)^* - (\Delta_1^Q)^* \Delta_2^Q)\right], \end{aligned} \quad (55)$$

There are no reasons to expect a non-zero  $\Psi$  on physics grounds, and to simplify the presentation, we set it to zero right away. The expectation value of  $\tilde{\Phi}$  is obviously non-zero, and this field has to be kept in the effective action.

Setting  $\Psi = 0$ , we re-write the partition function as

$$\begin{aligned} \mathcal{Z} &= \mathcal{Z}_0 \int d\Delta_1^Q d(\Delta_1^Q)^* d\Delta_2^Q d(\Delta_2^Q)^* \exp(-\alpha(|\Delta_1^Q|^2 + |\Delta_2^Q|^2)) \\ &\quad \times \int \frac{d\tilde{\Phi}}{\sqrt{8\pi\beta_1}} \exp\left(\frac{-\tilde{\Phi}^2}{8\beta_1}\right) \exp\left[i\tilde{\Phi}(|\Delta_1^Q|^2 + |\Delta_2^Q|^2)\right] \\ &\quad \times \int \frac{d\Upsilon}{\sqrt{4\pi\beta_1}} \exp\left(-\frac{\Upsilon^2}{4\beta_1}\right) \exp\left[i\Upsilon((\Delta_1^Q)^* \Delta_2^Q - \Delta_1^Q (\Delta_2^Q)^*)\right]. \end{aligned} \quad (56)$$

We next integrate out the fields  $\Delta_1^Q$  and  $\Delta_2^Q$  to obtain the effective action  $\mathcal{S}_{\text{eff}}[\tilde{\Phi}, \Upsilon]$ . Following the standard logics<sup>6</sup>, we extended  $\alpha$  to  $\alpha_q = \alpha + q^2$  to include spatial variations of fluctuating fields  $\Delta_1^Q$  and  $\Delta_2^Q$ . In principle, we also had to add the dynamical term to  $\alpha_q$ , but to analyze the transition at a finite  $T$  it is sufficient to consider only thermal fluctuations. With this extension, the expression for  $\mathcal{S}_{\text{eff}}[\tilde{\Phi}, \Upsilon]$  becomes

$$\mathcal{S}_{\text{eff}}[\tilde{\Phi}, \Upsilon] = T \int \frac{d^2q}{4\pi^2} \left\{ \frac{\tilde{\Phi}^2}{8\beta_1} + \frac{\Upsilon^2}{4\beta_1} + \log [(\alpha_q - i\tilde{\Phi})^2 - \Upsilon^2] \right\}. \quad (57)$$

We follow earlier works<sup>6,9,10</sup> and convert the field  $\tilde{\Phi}$  onto imaginary axis, i.e., introduce  $\Phi = -i\tilde{\Phi}$ . The action in terms of  $\Psi$  and  $\Upsilon$  is then

$$\mathcal{S}_{\text{eff}}[\Phi, \Upsilon] = T \int \frac{d^2q}{4\pi^2} \left\{ \frac{-\Phi^2}{8\beta_1} + \frac{\Upsilon^2}{4\beta_1} + \log [(\alpha_q + \Phi)^2 - \Upsilon^2] \right\}. \quad (58)$$

This is the Eq. (5) in the main text.

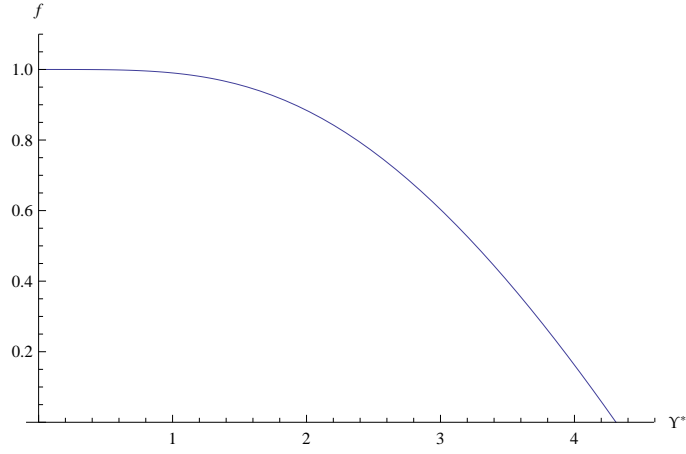


FIG. 11: The left hand side of Eq. (63) as a function of  $\Upsilon^*$

The saddle point of Eq. (57) is obtained by solving

$$\frac{\delta \mathcal{S}_{\text{eff}}}{\delta \Phi} = -\frac{\Phi}{4\beta_1} + 2 \int \frac{d^2 q}{4\pi^2} \frac{\alpha_q + \Phi}{(\alpha_q + \Phi)^2 - \Upsilon^2} = 0 \quad (59)$$

$$\frac{\delta \mathcal{S}_{\text{eff}}}{\delta \Upsilon} = \frac{\Upsilon}{2\beta_1} - 2 \int \frac{d^2 q}{4\pi^2} \frac{\Upsilon}{(\alpha_q + \Phi)^2 - \Upsilon^2} = 0. \quad (60)$$

We introduce  $r \equiv \alpha + \Phi$  and subsequently  $x \equiv q^2 + r$ , and obtain from Eq.(59):

$$\begin{aligned} r &= \alpha + \frac{2\beta_1}{\pi} \int_r^\Lambda \frac{dx x}{x^2 - \Upsilon^2} \\ &= \alpha + \frac{2\beta_1}{\pi} \log \frac{\Lambda}{\sqrt{r^2 - \Upsilon^2}}. \end{aligned} \quad (61)$$

From Eq. (60) we obtain the relation between  $\Upsilon$  and  $r$ :

$$1 = \frac{\beta_1}{\pi} \int_r^\infty \frac{dx}{x^2 - \Upsilon^2} = \frac{\beta_1}{\pi \Upsilon} \coth^{-1} \frac{r}{\Upsilon}. \quad (62)$$

Hence,  $r = \Upsilon \coth \pi \Upsilon / \beta_1$ . Plugging this into Eq. (61) and introducing  $\Upsilon^* \equiv \pi \Upsilon / \beta_1$  we obtain

$$\Upsilon^* \coth \Upsilon^* + 2 \log \frac{\Upsilon^*}{\sinh \Upsilon^*} = \alpha^*, \quad (63)$$

where  $\alpha^*$  is defined as

$$\alpha^* \equiv \frac{\pi}{\beta_1} \left( \alpha + \frac{2\beta_1}{\pi} \log \frac{\Lambda}{\beta_1} \right), \quad (64)$$

This is the Eq. (7) in the main text.

The variable  $\alpha^*$  changes sign at  $T = T_{\text{CDW}}$  and becomes negative at smaller  $T$ . If a solution of Eq. (63) with  $\Upsilon^* \neq 0$  emerges while  $\alpha^*$  is still positive, the system develops a preemptive collective instability at  $T = T^*$ , before the CDW order emerges. We plot the l.h.s. of Eq. (63) in Fig. 11. From the plot, we immediately see that a nonzero  $\Upsilon$  emerges through a second-order phase transition, when  $\alpha^*$  gets smaller than 1. Because  $\Upsilon$  couples linearly to  $i(\Delta_1^Q (\Delta_2^Q)^* - (\Delta_1^Q)^* \Delta_2^Q)$ , the emergence of a non-zero  $\Upsilon$  implies that  $\langle \Delta_1^Q (\Delta_2^Q)^* \rangle$  becomes non-zero and the expectation value is purely imaginary.

### C. Density component vs current component: going beyond hot spot approximation

So far, we assumed that CDW order parameter  $\Delta_k^Q$  is localized around hot spots, such that the pairs of hot spots (1,2) and (5,6) in Fig. 8 can be treated independent on each other. Within this approximation, the equations for

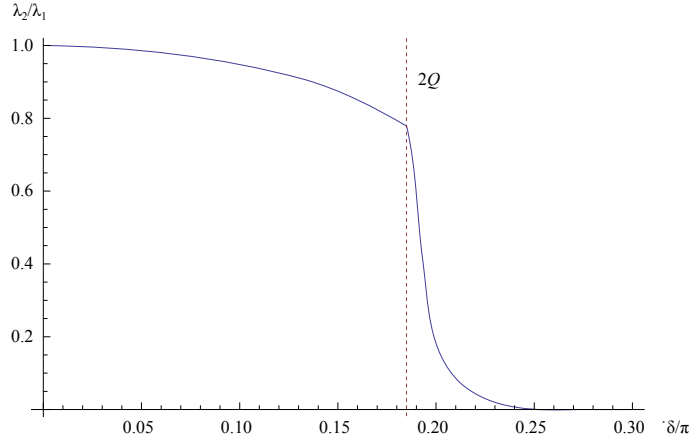


FIG. 12: The ratio of the eigenvalues  $\lambda_1$  and  $\lambda_2$  for even and odd in  $k$  CDW order parameters,  $\Delta_1^Q$  and  $\Delta_2^Q$ , respectively, as a function as the momentum integration range  $\delta$  of integration around the hot spots. Note the change of the behavior at  $\delta = 2Q$ . We set  $T = 1$  meV.

$\Delta_{k_0}^Q$  and  $\Delta_{-k_0}^Q$  decouple, and, as a result, the coefficient  $\alpha$  in the quadratic form in Eq. (48) is the same for the even component  $\Delta_1^Q$  and the odd component  $\Delta_2^Q$ . In reality, the integration over internal momenta in the equations for  $\Delta_{k_0}^Q$  and  $\Delta_{-k_0}^Q$  extends over some finite range around the hot spots, and the two regions somewhat overlap. Because the odd component of  $\Delta_k$  is absent when  $k_0$  and  $-k_0$  are equivalent points (say, when  $k_0 = (0, \pi)$ , as in the case of CDW with the diagonal momentum  $(Q, Q)$ ), it is natural to expect that overlapping favors the even solution over the odd solution, i.e., the prefactor for the even solution  $\Delta_1^Q$  changes sign, is larger than that for the odd solution. This behavior has been obtained in Ref. [11], where the authors restricted with the first lattice harmonics for  $\Delta$ , e.g., approximated  $\Delta_1^Q$  by  $\cos k_x \cos Q_y$  (for our choice of stripe order) and  $\Delta_2^Q$  by  $\sin k_x \sin Q_y$ . In our approach, we expand near hot spots, what in lattice notations means that our  $\Delta_1^Q$  and  $\Delta_2^Q$  are constructed out of many lattice harmonics. Still, we expect the same trend as in<sup>11</sup> – larger eigenfunction for the even solution. To verify this, we approximate the interaction  $\bar{\chi}(\mathbf{k}, \mathbf{k}')$  as a constant within some small momentum window  $\pi - \delta < k'_x - k_x < \pi + \delta$  and  $\pi - \delta < k'_y - k_y < \pi + \delta$ , and set it to zero outside this window. The two eigenvalues are explicitly expressed as

$$\begin{aligned} \lambda_1 &= \frac{\bar{\chi}^2}{\Delta_1^Q(k_0)} \int_{-\delta}^{\delta} \frac{dp f(\epsilon_{k_\pi+p+Q}) - f(\epsilon_{k_\pi+p-Q})}{\epsilon_{k_\pi+p-Q} - \epsilon_{k_\pi+p+Q}} \int_{-\delta}^{\delta} \frac{dq f(\epsilon_{k_0+p+q+Q}) - f(\epsilon_{k_0+p+q-Q})}{\epsilon_{k_0+p+q-Q} - \epsilon_{k_0+p+q+Q}} \Delta_1^Q(k_0 + p + q) \\ \lambda_2 &= \frac{\bar{\chi}^2}{\Delta_2^Q(k_0)} \int_{-\delta}^{\delta} \frac{dp f(\epsilon_{k_\pi+p+Q}) - f(\epsilon_{k_\pi+p-Q})}{\epsilon_{k_\pi+p-Q} - \epsilon_{k_\pi+p+Q}} \int_{-\delta}^{\delta} \frac{dq f(\epsilon_{k_0+p+q+Q}) - f(\epsilon_{k_0+p+q-Q})}{\epsilon_{k_0+p+q-Q} - \epsilon_{k_0+p+q+Q}} \Delta_2^Q(k_0 + p + q), \end{aligned} \quad (65)$$

where  $f(\epsilon)$  is the Fermi function. We approximate the odd and even solutions as

$$\begin{aligned} \Delta_1^Q(k) &\approx \text{const.} \\ \Delta_2^Q(k) &\approx 2\pi - (k_x + k_y). \end{aligned} \quad (66)$$

We evaluated the two integrals numerically using the dispersion relation for  $\text{Pb}_{0.55}\text{Bi}_{1.5}\text{Sr}_{1.6}\text{La}_{0.4}\text{CuO}_{6+\delta}$  (see Ref. [12]). In Fig. 12 we show our results for  $\lambda_2/\lambda_1$  as a function of the momentum window size  $\delta$ .

We see from the plot that, as expected,  $\lambda_2 < \lambda_1$ , i.e., the even solution emerges at a higher  $T$ , although number-wise the values of  $\lambda_2$  and  $\lambda_1$  are quite close as long as  $\delta < 2Q$ . That  $\lambda_1$  is larger, but  $\lambda_2$  is close second is consistent with Ref. [11]. If there was no preemptive transition, this result would imply that only  $\Delta_1$  emerges at  $T_{\text{CDW}}$ , and  $\Delta_2$  potentially appears at a lower  $T$ . As we discuss in the main text, the preemptive transition forces the two orders to appear simultaneously, if  $T^* - T_{\text{CDW}}$  exceeds the difference between CDW transition temperatures for even and odd CDW order parameters.

## VIII. COMPARISON WITH ARPES DATA

In this section we discuss in some detail the comparison between our theory and ARPES data. Numerous ARPES data on the fermionic spectral function in the pseudogap region show<sup>12–16</sup> that below  $T^*$ , the spectral weight in the

antinodal regions gets transformed to higher frequencies, and the FS effectively takes the form of the Fermi arcs. We show below that this is expected behavior for a system with strong CDW fluctuations, but without a true CDW order.

A generic charge order with an ordering momentum  $Q$  introduces a new term  $H' = \Delta_k^Q c_{k+Q}^\dagger c_{k-Q} + h.c.$  into the Hamiltonian. Then fermions with momenta  $k \pm Q, k \pm 3Q, k \pm 5Q, \dots$  all become coupled. For commensurate  $Q = \pi M/(N)$ , where  $M$  and  $N$  are integers, the ‘‘chain’’ of coupled momenta gets closed when after  $N$  steps, for incommensurate  $Q$  it is not closed, strictly speaking, but for practical purposes one can approximate  $Q$  by a close commensurate value. To diagonalize such a Hamiltonian one has to solve a  $N$ -dimensional matrix equation<sup>11</sup>. The energy eigenstates with eigenvalues  $E_1, E_2, \dots, E_N$  are linear combinations of the original fermions,

$$\begin{pmatrix} d_1 \\ d_2 \\ \vdots \\ d_N \end{pmatrix} = \begin{pmatrix} u_{11} & u_{12} & \cdots & u_{1N} \\ u_{21} & u_{22} & \cdots & u_{2N} \\ \vdots & \vdots & \ddots & \vdots \\ u_{N1} & u_{N2} & \cdots & u_{NN} \end{pmatrix} \begin{pmatrix} c_k \\ c_{k-2Q} \\ \vdots \\ c_{k-2(N-1)Q} \end{pmatrix}, \quad (67)$$

The ARPES spectral function measures the correlator of  $c$ -fermions and contains contributions from all edentates, with different weights

$$\begin{aligned} I(\omega, k) &\propto \text{Im}(\langle c_k(\omega) c_k^\dagger(\omega) \rangle) \\ &= \text{Im} \left( \sum_i u_{i1}^2 \langle d_i(\omega) d_i^\dagger(\omega) \rangle \right) = \text{Im} \left( \sum_i \frac{u_{i1}^2}{\omega - E_i - i\Gamma} \right), \end{aligned} \quad (68)$$

where  $\Gamma$  is kept as a finite lifetime to model the state below  $T^*$ , in which CDW fluctuations are well-developed but a true CDW order does not yet occur. Using this procedure, we computed the spectral function  $I(\omega, k)$  at  $\omega = 0$ , as a function of  $k$  for stripe CDW order with either  $Q = Q_x$  or  $Q = Q_y$ . The position of the peak in this spectral function yields the location of the reconstructed FS in the non-superconducting state. Since in a macroscopic system there exist domains with stripes in both directions, ARPES should measure the contributions from both. To model this, we assume that the measured ARPES intensity is the sum of  $I(\omega, k)$  for  $Q = Q_x$  and  $Q = Q_y$ . Combining the spectral functions for CDW orders with  $Q_x$  and  $Q_y$ , we obtained Fig. 4(a) in the main text. The Fermi arcs, terminating at hot spots, are clearly visible. The actual FS's in the CDW-ordered state indeed cannot terminate inside the BZ, but other pieces of the FS have small spectral weights and are washed out by a finite  $\Gamma$ . In the calculations we used the dispersion from Ref. [12]:  $\epsilon(k_x, k_y) = -2t(\cos k_x + \cos k_y) - 4t'(\cos k_x \cos k_y) - 2t''(\cos 2k_x + \cos 2k_y) - 4t'''(\cos 2k_x \cos k_y + \cos k_x \cos 2k_y) - \epsilon_0$ , with  $t = 0.22eV$ ,  $t' = -0.034315eV$ ,  $t'' = 0.035977eV$ ,  $t''' = -0.0071637eV$ , and we took  $\epsilon_0 = -0.24327eV$ , slightly different from  $-0.240577eV$  in [12], to get a commensurate  $2Q = 0.2\pi$  instead of  $2Q \approx 0.19\pi$  in [12]. We then used  $N = 10$ ,  $M = 1$ , and set  $\Gamma = 50meV$ .

The physical origin of the arc behavior can be understood analytically. Taking  $Q = Q_y$  and the region around hot spot 1 in Fig. 8, with momenta near  $k_0 + Q$ , one can verify that the most relevant mixing, introduced by CDW order, is the one which involves the momenta  $k_0 + Q$  and  $k_0 - Q$ , since for the rest the gap function is much smaller, and also high-energy fermionic states are involved. The effective  $2 \times 2$  Hamiltonian  $H = H_0 + H'$  can then be diagonalized by the standard Bogoliubov transformation. Defining  $c_1 = c_k$ ,  $c_2 = c_{k-2Q}$ ,  $\epsilon_1 = \epsilon_k$ ,  $\epsilon_2 = \epsilon_{k-2Q}$ , and  $\Delta = |\Delta_{k_0}^Q|$ , we obtain

$$\begin{pmatrix} d_+ \\ d_- \end{pmatrix} = \begin{pmatrix} u & v \\ -v & u \end{pmatrix} \begin{pmatrix} c_1 \\ c_2 \end{pmatrix}, \quad (69)$$

where

$$\begin{aligned} u^2 &= \frac{1}{2} \left[ 1 + \frac{\epsilon_1 - \epsilon_2}{\sqrt{(\epsilon_1 - \epsilon_2)^2 + 4\Delta^2}} \right] \\ v^2 &= \frac{1}{2} \left[ 1 - \frac{\epsilon_1 - \epsilon_2}{\sqrt{(\epsilon_1 - \epsilon_2)^2 + 4\Delta^2}} \right], \end{aligned} \quad (70)$$

with energy eigenvalues

$$E_{\pm} = \frac{\epsilon_1 + \epsilon_2}{2} \pm \sqrt{\left(\frac{\epsilon_1 - \epsilon_2}{2}\right)^2 + \Delta^2}. \quad (71)$$

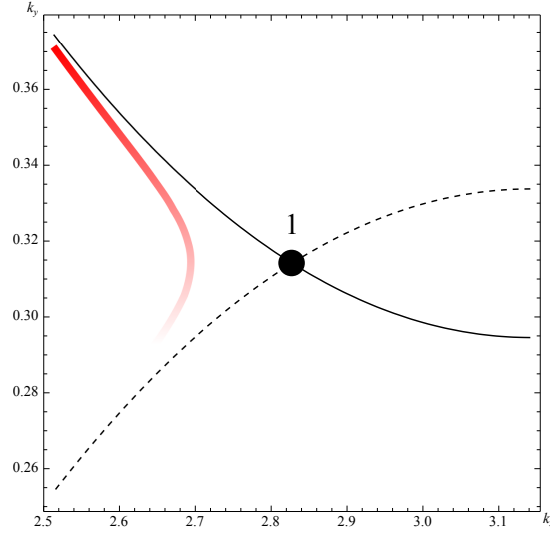


FIG. 13: The position of the peak in spectral function at  $\omega = 0$  around the hot spot 1 (red line). The saturation of color indicates the spectral weight of the peak. The spectrum to the right of the hot spot 1 is pushed out of BZ boundary by large enough CDW order parameter  $\Delta$  used in the plot.

the ARPES spectral function at  $\omega = 0$  is

$$I(\omega = 0, k) \propto \text{Im}(\langle c_1 c_1^\dagger \rangle) = \text{Im} \left( \frac{u^2}{E_+ - i\Gamma} + \frac{v^2}{E_- - i\Gamma} \right). \quad (72)$$

The peaks in the momentum distribution curves are at  $E_{\pm} = 0$ , which correspond to  $\epsilon_1 \epsilon_2 = \Delta^2$ . This condition defines a hyperbola in the momentum space around the hot spot 1, as shown in Fig. 13. The solid and dashed lines in this figure are the original FS  $\epsilon_k = 0$  and the “shadow” FS  $\epsilon_{k-2Q} = 0$ . At small  $\Delta$ , there is another part of the FS, to the right of point 1 in this figure, but for large enough  $\Delta$  used in the plot the right branch is pushed out the BZ boundary. The spectral weight along the red line in Fig. 13 depends on coherence factors and is much larger for the part that is close to the original FS, than for the part close to the shadow FS. As a result, the only visible spectral peak at  $\omega = 0$  in the momentum space is along the former FS  $\epsilon_k = 0$ , and it effectively terminates at the hot spot, as in Fig. 13. The contribution from the domain with  $Q = Q_x$  is obtained in a similar manner, and the full result is the spectral function with largest intensity at four Fermi arcs, as in Fig. 4(a) in the main text.

Another focus of our interest is the measured ARPES dispersion along the BZ boundary in the antinodal (AN) regions. Experiments<sup>12</sup> performed on  $\text{Pb}_{0.55}\text{Bi}_{1.5}\text{Sr}_{1.6}\text{La}_{0.4}\text{CuO}_{6+\delta}$  (Pb-Bi2201) have detected two prominent features: (1) upon cooling below  $T^*$ , the momentum at which the dispersion has a minimum shifts from  $k_F$  to a larger value  $k_G$ , (2) at  $T < T_c$ , there emerges a weak, “shoulder”-like peak in the energy distribution curve at the binding energy  $\omega \sim 30$  meV. We find that both these features can be accounted for within our theory.

Again, we need to consider two domains: domain I with CDW order along  $y$  direction, and domain II with CDW order along  $x$  direction. For simplicity, we will assume both CDW gap functions can be approximated by constants, in which case  $\Delta_x = \mu \Delta_y$ , with  $\mu > 1$ . Because typical energy scale for fermionic dispersion in the AN region, albeit larger than  $\Gamma$ , is much smaller than the bandwidth, we again can neglect high-energy electronic states. A simple analysis shows that for low-energy consideration it is sufficient to include three states with momenta  $k, k + 2Q_{y,x}, k - 2Q_{y,x}$ . We show this in Fig. 14 (a) and 14 (b).

In domain I, the two states with momenta  $k$  and  $k + 2Q_y$  cross at a small positive energy  $\delta\epsilon$  near the  $\mathbf{k}_F$  point along the BZ boundary ( $\mathbf{k}_F = (k_x, \pi)$ ). The energy of the state with momentum  $k - 2Q_y$  is much larger in this region. In this situation, we can further reduce the three-state system it to a two-state system. The energy eigenvalues at the crossing point are  $\delta\epsilon \pm \Delta_y$ . Once  $\Delta_y$  exceeds  $\delta\epsilon$ , one of the energies  $E_1 = \delta\epsilon - \Delta_y < 0$  becomes negative, and the corresponding state becomes visible by ARPES. Carrying out calculations at different  $k$ , we found that this  $E_1$  sets the local minimum of the reconstructed dispersion. We show this in Fig. 14 (a). Most importantly, this local minimum is reached at  $k = k_G \equiv Q$ , which is necessary larger than  $k_F$ . As a result, the position of the minimum shifts from  $k_F$  to a larger value  $k_G$ . We stress that this happens because the order is along  $Q_y$  (in our geometry). For CDW order with diagonal momentum ( $\pm 2Q, \pm 2Q$ ), we found the opposite result: the position of the local minimum shifts to a smaller momentum. This would contradict the experiment.

We used the experimental values of  $\epsilon_a(k_y = 0) = -38$  meV,  $\epsilon_b = -59$  meV, and  $\delta\epsilon = 5$  meV, and set  $\Delta_y = 35$  meV



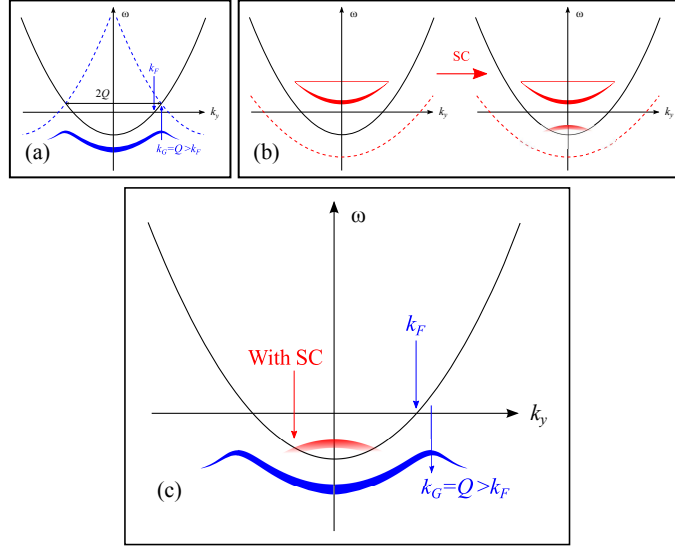


FIG. 14: Interpretation of the ARPES data around antinodal areas. Panel (a) – contribution from the domain I with  $Q = Q_y$ . Panel (b) – contribution from the domain II with  $Q = Q_x$ . Panel (c) – The combined spectral peaks from both domains seen by ARPES.

to match the energy of the local minima at  $k_G$  at  $\omega = 30$  meV in<sup>12</sup>. Using these numbers, we obtained rather good agreement with the full reconstructed spectrum.

In domain II, two out of three states are degenerate, and we define  $\epsilon_{\pi+2Q,k_y} = \epsilon_{\pi-2Q,k_y} \equiv \epsilon_b(k_y)$ . We also define  $\epsilon_a(k_y) = \epsilon_{\pi,k_y}$ . By solving such a 3-by-3 matrix equation on eigen-values and eigen-functions we find that the dominant contribution to the spectral function comes from  $E_1 = (\epsilon_a + \epsilon_b)/2 + \sqrt{[(\epsilon_a - \epsilon_b)/2]^2 + 2\Delta_x^2} > \epsilon_a$ . We note that  $\epsilon_a = -38$  meV is small and  $\Delta_x > \Delta_y = 35$  meV. For such parameters, we found that  $E_1 > 0$ . Since ARPES can only detect filled states, the peak at  $E_1 > 0$  is invisible to ARPES. In other words, in the normal state, the full dispersion measured by ARPES comes from domain I.

Once superconductivity sets in at  $T_c$ , electron and hole states mix up, and the system develops a shadow image of  $E_1$  at a negative energy, at  $-\sqrt{E_1^2 + \Delta_{sc}^2}$ . The superconducting gap  $\Delta_{sc}$  is rather small in Pb-Bi2201, hence the image is at approximately  $-E_1$ . We show this in Fig. 14 (b). Like we said, the emergence of the new flat dispersion below  $T_c$  has been observed in the experiment<sup>12</sup>. The position of the new band is at around 25 meV. To match it, we need  $\Delta_x = 51$  meV, consistent with  $\Delta_x = \mu\Delta_y$  and  $\mu > 1$ , although we were not able to extract the value of  $\mu$  from the data.

In Fig. 14 (c) we show the combined peaks from both domains. This is our theoretical result for the spectral function for comparison with ARPES. We view the agreement with the data as reasonably good.

## IX. BOND ORDER WITH DIAGONAL MOMENTA $(\pm Q, \pm Q)$

For completeness and for comparison with our results on CDW order with  $Q_x$  or  $Q_y$ , we also consider charge order with momenta  $\bar{\mathbf{Q}} = (\pm Q, \pm Q)$ , as depicted in Fig. 15. A charge order with diagonal momentum has been studied in Refs. [3,17]. The critical temperature for the instability towards such order is exactly the same as superconducting  $T_c$ , if one neglects the curvature of the FS near the hot spots. The gap function for a diagonal charge order has a  $d$ -wave structure  $\langle c^\dagger(k + \bar{Q}/2)c(k - \bar{Q}/2) \rangle = \Delta(\cos k_x - \cos k_y)$ , similar to that of a  $d$ -wave superconducting order parameter. A  $d$ -wave charge order does not create a charge density modulation  $\langle c^\dagger(r)c(r) \rangle$ , but it introduces modulations of the correlation function between neighboring sites:

$$\langle c^\dagger(\mathbf{r})c(\mathbf{r} + \mathbf{a}) \rangle = 2\Delta \cos \bar{\mathbf{Q}} \cdot \left( \mathbf{r} + \frac{\mathbf{a}}{2} \right) (\delta_{\mathbf{a},\mathbf{x}} - \delta_{\mathbf{a},\mathbf{y}}) \quad (93)$$

where  $\mathbf{x}$  and  $\mathbf{y}$  are vectors along  $x$  and  $y$  directions, in units of interatomic spacing  $\mathbf{a}$ . A charge order of this kind is called bond order.

To obtain the onset temperature for bond order,  $T_{BO}$ , and compare it with superconducting  $T_c$ , we add to the spin-fermion action two infinitesimal vertices  $\Phi_0(k)c_{k,\alpha}(i\sigma_{\alpha\beta}^y)c_{-k,\beta}$  and  $\Psi_0(k)c_{k,\alpha}\delta_{\alpha\beta}c_{k+\bar{Q},\beta}^\dagger$ , where  $k$  stands for  $2+1$

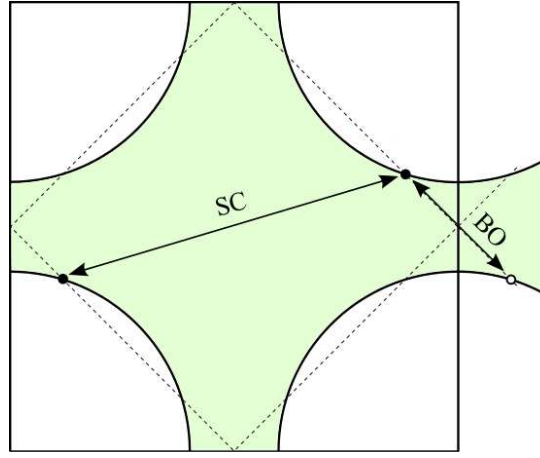


FIG. 15: Fermions which contribute to diagonal bond order and  $d$ -wave superconducting order. Filled and empty circles denote particle and hole states, respectively.

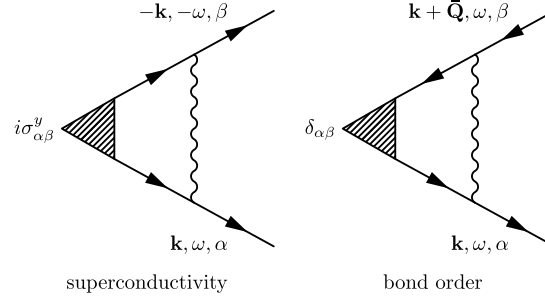


FIG. 16: The diagrammatic expressions for the fully renormalized vertices in superconducting and bond order channels.

momentum  $(\omega_m, \mathbf{k})$ . These vertices get renormalized by spin-fermion interaction, and the critical temperature ( $T_{\text{BO}}$  or  $T_c$ ) is obtained when the corresponding susceptibility diverges, i.e., the solution for fully renormalized  $\Phi(k)$  or  $\Psi(k)$  exists even when the bare vertices are set to zero.

The authors of [3,17] have demonstrated that a superconducting instability and an instability towards bond order come from the fermions located in the same hot regions, only for bond order one of the regions is shifted by  $(2\pi, 0)$ . The ladder renormalizations of  $\Phi_0(k)$  and  $\Psi_0(k)$  are shown in Fig. 16, where the wavy line is the spin-fermion interaction. In analytical form we have, at the corresponding critical temperatures,

$$\begin{aligned}\Phi(k) &= -3 \int G(k')G(-k')\chi(k-k')\Phi(k'+\pi) \\ \Psi(k) &= 3 \int G(k')G(k+\bar{Q})\chi(k-k')\Psi(k'+\pi),\end{aligned}\quad (74)$$

where  $\chi(k-k')$  is defined in the main text and in the first Section of the SM. The difference in the overall sign in the r.h.s is due to different Pauli algebra – for superconducting vertex  $\sigma_{\alpha'\alpha}^i(i\sigma_{\alpha\beta}^y)\sigma_{\beta\beta'}^i = -3i\sigma_{\alpha'\beta'}^y$ , while for bond vertex  $\sigma_{\alpha'\alpha}^i(\delta_{\alpha\beta})\sigma_{\beta\beta'}^i = 3\delta_{\alpha'\beta'}$ . One can easily verify that, if one neglects the curvature of the FS,  $\epsilon_{k+\bar{Q}} = -\epsilon_k$ , and hence  $G(-k) = -G(k+\bar{Q})$ . In this approximation, the two channels are then degenerate<sup>3</sup>, i.e.,  $T_c = T_{\text{BO}}$ . Once the curvature of the FS is included, the degeneracy is lifted and  $T_c > T_{\text{BO}}$ . The reasoning here is that superconductivity involves fermions with strictly opposite  $k$ , and the momentum integration can still be replaced by the integration over  $\epsilon_k$ , with a constant prefactor, even in the presence of the FS curvature. For bond order, the relation  $\epsilon_{k+\bar{Q}} = -\epsilon_k$  no longer holds in the presence of the FS curvature, and this reduces the kernel in the Eq. (74) for  $\Psi$ .

Explicitly, expanding near a hot spot, we obtain

$$\epsilon(k) = -v_F(k_\perp + \tilde{\kappa}k_\parallel^2/k_F), \quad (75)$$

where  $k_\parallel$  and  $k_\perp$  are momenta parallel and perpendicular to the FS, respectively, and  $\tilde{\kappa}$  is a dimensionless parameter

characterizing the curvature of the FS. In this section we will use dimensionless parameters

$$\begin{aligned}\tilde{g} &\equiv \frac{\bar{g}}{v_F k_F} \\ \tilde{\xi} &\equiv \xi k_F.\end{aligned}\tag{76}$$

where  $\xi$  is the magnetic correlation length. The dimensionless coupling  $\tilde{g}$ , dimensionless correlation length  $\tilde{\xi}$ , and dimensionless FS curvature  $\tilde{\kappa}$  are three input parameters for the consideration in this Section. An additional parameter, set by the FS geometry, is the angle between Fermi velocities at hot spots separated by  $(\pi, \pi)$ . To simplify the presentation, we assume that these two velocities are orthogonal to each other.

We follow earlier works<sup>1-3,17-19</sup> and assume that the spin-fermion interaction can be well approximated by its value between fermions on the FS. Integrating over momenta transverse to the FS in the fermionic propagators, we obtain integral equations for  $\Phi(\omega_m, k_{\parallel})$  and  $\Psi(\omega_m, k_{\parallel})$ , which depend on frequency and on momenta along the FS. The equations are

$$\Phi(\omega_m, k_{\parallel}) = \int_{m'k'_{\parallel}} K(\omega_m, k_{\parallel}, \omega'_m, k'_{\parallel}; 0) \Phi(\omega'_m, k'_{\parallel}),\tag{77}$$

$$\Psi(\omega_m, k_{\parallel}) = \int_{m'k'_{\parallel}} K(\omega_m, k_{\parallel}, \omega'_m, k'_{\parallel}; \tilde{\kappa}) \Psi(\omega'_m, k'_{\parallel}),\tag{78}$$

where  $\int_{m'k'_{\parallel}}$  stands for  $T \sum_{m'} \int dk'_{\parallel}/2\pi$  and

$$K(\omega_m, k_{\parallel}, \omega'_m, k'_{\parallel}; \tilde{\kappa}) = \frac{3\tilde{g}k_F/2 |\omega'_m + \Sigma(\omega'_m, k'_{\parallel})|}{[\omega'_m + \Sigma(\omega'_m, k'_{\parallel})]^2 + v_F^2 \tilde{\kappa}^2 k_{\parallel}^4 / k_F^2} \frac{1}{k_{\parallel}^2 + k_{\parallel}'^2 + \gamma|\omega_m - \omega'_m| + \tilde{\xi}^{-2} k_F^2}\tag{79}$$

#### A. $T_c$ and $T_{\text{BO}}$ at the onset of SDW order

At the magnetic quantum-critical point  $\tilde{\xi}^{-1} = 0$ . We show that, in this situation, the critical temperature for bond order  $T_{\text{BO}}$  is smaller than  $T_c$  due to curvature. This agrees with earlier works<sup>3,17</sup>. That  $T_{\text{BO}} < T_c$  can be seen directly from Eq (79) because the kernel  $K$  is positively definite and is suppressed in the presence of  $\tilde{\kappa}$ . However, we also show that, at  $\tilde{\xi}^{-1} = 0$ ,  $T_{\text{BO}}$  remains non-zero even if the curvature is large.

It is convenient to introduce the set of rescaled variables

$$\bar{T} = \frac{\pi T}{\omega_0}, \quad \bar{\omega}_m = \frac{\omega_m}{\omega_0}, \quad \bar{k}_{\parallel} = \frac{k_{\parallel}}{\sqrt{\gamma\omega_0}}.\tag{80}$$

In these notations, the linearized gap equation for the bond order becomes

$$\Psi(\bar{\omega}_m, \bar{k}_{\parallel}) = \frac{1}{4\pi} \int_{\bar{T}} \frac{d\bar{\omega}_m d\bar{k}'_{\parallel}}{\bar{k}_{\parallel}^2 + \bar{k}'_{\parallel}{}^2 + |\bar{\omega}_m - \bar{\omega}'_m|} \frac{|\bar{\omega}'_m + \bar{\Sigma}(\bar{\omega}'_m, \bar{k}'_{\parallel})|}{|\bar{\omega}'_m + \bar{\Sigma}(\bar{\omega}'_m, \bar{k}'_{\parallel})|^2 + 16\tilde{g}^2 \tilde{\kappa}^2 \bar{k}'_{\parallel}{}^4 / \pi^2} \Psi(\bar{\omega}'_m, \bar{k}'_{\parallel}),\tag{81}$$

where the rescaled self-energy is<sup>2,3</sup>

$$\bar{\Sigma}(\bar{\omega}_m, \bar{k}_{\parallel}) = \sqrt{|\bar{\omega}_m| + \bar{k}_{\parallel}^2} - |\bar{k}_{\parallel}|.\tag{82}$$

We verified, using the same strategy as in our earlier work<sup>4</sup> on superconducting  $T_c$  at  $\tilde{\xi}^{-1} = 0$ , that the leading contribution to the r.h.s of Eq. (81) comes from the region where  $\bar{\Sigma} > \bar{\omega}'_m$  and  $\bar{k}_{\parallel}^2 > \bar{\omega}$ . In this region, the momentum dependence of  $\Psi$  is more relevant than its frequency dependence. Keeping only the momentum dependence in  $\Psi$  and introducing  $x = \bar{k}_{\parallel}^2$  and  $y = \bar{k}$ , we re-write (81) as

$$\Psi(y) = \frac{1}{2\pi} \int_{\bar{T}_{\text{BO}}}^1 \frac{dx}{x+y} \log \frac{x^2 + 64\tilde{g}^2 \tilde{\kappa}^2 x^3}{\bar{T}^2 + 64\tilde{g}^2 \tilde{\kappa}^2 x^3} \Psi(x).\tag{83}$$

For superconductivity, the same procedure yields

$$\Phi(y) = \frac{1}{\pi} \int_{\bar{T}_c}^1 \frac{dx}{x+y} \log \frac{x}{\bar{T}} \Phi(x).\tag{84}$$

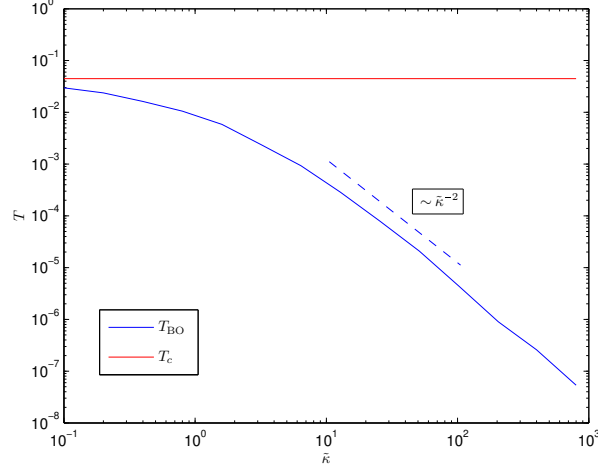


FIG. 17: The onset temperatures for superconductivity and bond order,  $T_c$  and  $T_{\text{BO}}$ , respectively as functions of dimensionless FS curvature  $\tilde{\kappa}$  at the onset of SDW order (magnetic  $\xi^{-1} = 0$ ). We set  $\tilde{g} = 0.1$ . Superconducting  $T_c$  is not affected by the curvature, while  $T_{\text{BO}}$  decreases but remains finite. In analytical consideration  $T_{\text{BO}}/T_c$  was found to scale as  $\tilde{\kappa}^{-2}$  at large enough curvature. We show this functional behavior by a dashed line.

Comparing Eqs. (83) and (84), we find that the curvature term couples to  $x^3$  and provides a soft *upper* cutoff to the integral over  $x$ , at  $x \sim 1/(\tilde{g}\tilde{\kappa})^2$ . At large  $\tilde{g}\tilde{\kappa}$  we then have  $T_{\text{BO}}/T_c \propto 1/(\tilde{g}\tilde{\kappa})^2 \ll 1$ . We see that  $T_{\text{BO}}$  remains finite, no matter how strong the curvature is. In other words, at  $\xi^{-1} = 0$ , there is no threshold value of  $\tilde{\kappa}$  above which bond order would not develop.

To check our analytical reasoning, we solved Eqs (77) and (78) numerically and obtained the same result –  $T_{\text{BO}}$  decreases with increasing  $\tilde{\kappa}$ , but remains finite. We show the results in Fig. 17. We set  $\tilde{g} = 0.1$ ,  $\tilde{\xi} = \infty$ , and varied  $\tilde{\kappa}$ .

### B. $T_c$ and $T_{\text{BO}}$ at a finite $\tilde{\xi}$

When the system moves away from the magnetic QCP, it eventually recovers a conventional FL behavior in the normal state. Indeed, as the correlation length  $\tilde{\xi}$  decreases,  $\omega_{sf} = \tilde{\xi}^{-2}k_F^2/\gamma$  becomes the upper energy cutoff for the pairing<sup>2,20</sup>. Below this scale, the spin susceptibility can be treated as frequency-independent constant and the fermionic self-energy is linear in frequency:

$$\begin{aligned} \Sigma(\omega_m, k_{\parallel}) &= \frac{3\tilde{g}k_F}{2\pi\sqrt{\gamma}} \left( \sqrt{|\omega_m| + k_{\parallel}^2/\gamma + \omega_{sf}} - \sqrt{k_{\parallel}^2/\gamma + \omega_{sf}} \right) \text{sgn}(\omega_m) \\ &\approx \frac{3\tilde{g}\tilde{\xi}\sqrt{\omega_{sf}}}{2\pi} \frac{\omega_m}{2\sqrt{\omega_{sf}}} \\ &= \lambda\omega_m. \end{aligned} \quad (85)$$

In the last line we have defined  $\lambda = \frac{3\tilde{g}\tilde{\xi}}{4\pi}$ . Plugging this into Eq. (77) for superconducting  $T_c$  and using the condition that typical  $\omega, \omega'_m, k_{\parallel}^2, k'_{\parallel}{}^2/\gamma$  are all small in this limit compared to  $\omega_{sf}$ , we integrate over momentum  $k'_{\parallel}$  and obtain

$$\Phi = \frac{\lambda}{1+\lambda} \log \frac{\omega_{sf}}{T} \Phi. \quad (86)$$

For superconducting  $T_c$  we then have a conventional BCS-McMillan result<sup>21</sup>

$$T_c \sim \omega_{sf} \exp\left(-\frac{1+\lambda}{\lambda}\right). \quad (87)$$

Hence, as the system moves away from the QCP, it crosses over to a BCS behavior, and  $T_c$  gradually decreases as  $\tilde{\xi}$  decreases and  $\lambda$  gets smaller.

For bond order, the gap equation in the rescaled variables becomes, in this limit,

$$\Psi = \frac{1}{4\pi} \int_{\bar{T}} \frac{d\omega_m d\bar{k}'_{\parallel}}{\bar{k}'_{\parallel}{}^2 + \tilde{\omega}_{sf}} \frac{(1+\lambda)|\tilde{\omega}'_m|}{(1+\lambda)^2|\tilde{\omega}'_m|^2 + 16\tilde{g}^2\tilde{\kappa}^2\bar{k}'_{\parallel}{}^4/\pi^2} \Psi, \quad (88)$$

where we defined

$$\tilde{\omega}_{sf} \equiv \frac{\omega_{sf}}{\omega_0} = (2\lambda)^{-2}. \quad (89)$$

Typical  $\bar{k}'_{\parallel}{}^2$  are of order  $\tilde{\omega}_{sf}$ , and in the second term in the denominator we can safely replace  $\bar{k}'_{\parallel}{}^4$  by  $\tilde{\omega}_{sf}^2$ . We then see that the curvature  $\tilde{\kappa}$  now appears in a combination with a constant term and by this reason provides a *lower* cutoff for the BCS-like logarithmic behavior. This is qualitatively different from the behavior at the magnetic QCP, where the curvature couples to the running variable  $x^3$ . Because of the cutoff, the frequency integral no longer diverges at  $T = 0$ . Hence, at some critical  $\tilde{\xi}$ , the linearized gap equation for bond-order vertex has a solution at  $T = 0$ . Explicitly setting  $T = 0$  in (88) and integrating over  $\bar{k}'_{\parallel}$ , we obtain,

$$\Psi = \frac{1}{2} \frac{\lambda\Psi}{1+\lambda} \int_{-\omega_{sf}}^{\omega_{sf}} \frac{d\omega |\omega|}{|\omega|^2 + 16\tilde{g}^2\tilde{\kappa}^2\omega_{sf}^2/\pi^2}. \quad (90)$$

Integrating over frequency, we find

$$1 = \frac{\lambda}{1+\lambda} \left( \log \frac{\pi}{4\tilde{g}\tilde{\kappa}} \right). \quad (91)$$

The solution exists at the critical  $\tilde{\xi}$  given by

$$\tilde{\xi}_{cr}^{-1} \sim \tilde{g} \log \left( \frac{\pi}{4\tilde{g}\tilde{\kappa}} \right). \quad (92)$$

At smaller  $\tilde{\xi} < \tilde{\xi}_{cr}$ , the equation on  $\Psi$  only allows a trivial solution  $\Psi = 0$ , hence bond order does not develop at any  $T$ .

To verify this, we solved for  $T_c$  and  $T_{BO}$  numerically. We set  $\tilde{g} = 0.1$  and  $\tilde{\kappa} = 0.14$  and varied  $\tilde{\xi}$ . We verified that superconducting  $T_c$  crosses over to BCS behavior at small enough  $\tilde{\xi}$ , while for bond order, there exists a critical  $\tilde{\xi}$  at which  $T_{BO}$  vanishes. We show the results in Fig. 18.

Although the behavior of  $T_{BO}$  resembles that of  $T_{CDW}$  for CDW order with either vertical or horizontal  $\mathbf{Q}$ , the physics behind the reduction of these temperatures with decreasing magnetic  $\xi$  is different. For bond order with diagonal  $\mathbf{Q}$ , the reduction of  $T_{BO}$  compared to  $T_c$  and its eventual vanishing is solely due to the FS curvature. If we set  $\tilde{\kappa}$  to zero,  $T_c$  and  $T_{BO}$  remain identical at any  $\xi$ . For CDW order with vertical or horizontal  $\mathbf{Q}$ , the reduction and eventual vanishing of  $T_{CDW}$  upon decreasing of  $\tilde{\xi}$  is not related to curvature and holds even if we set curvature to zero. At a small curvature then,  $T_{BO} > T_{CDW}$ , but which temperature is larger at  $\tilde{\kappa} = O(1)$  depends on numbers. We emphasize again in this regard that for CDW with a vertical or horizontal  $\mathbf{Q}$ , the first instability upon lowering  $T$  is at  $T^* > T_{CDW}$ , towards the state which breaks time-reversal symmetry. No such transition holds for bond order with a diagonal  $\mathbf{Q}$ .

### C. Interplay between superconductivity and bond order

For completeness, we also present the phase diagram for the (artificial) case when the only two competing states are superconductivity and bond order with a diagonal  $\mathbf{Q}$ , i.e. when CDW order with vertical or horizontal  $\mathbf{Q}$  is just neglected. We show the result in Fig. 19. Because  $T_c$  is larger than  $T_{BO}$ , the leading instability upon lowering  $T$  is always into a superconducting state, bond order may appear only at a lower  $T$ . At the same time, at large  $\xi$ ,  $T_c$  by itself is reduced because over some range of  $T$  the system fluctuates between superconductivity and bond order<sup>11,17</sup> (a light blue region in Fig. 19). The phase diagram in Fig. 19 is similar to that in Ref. [17], but differs in that in our analysis bond order only emerges at  $\tilde{\xi} > \tilde{\xi}_{cr}$ , i.e., there exists another quantum-critical point (QCP<sub>2</sub>) at some distance away from a magnetic quantum-critical point (QCP<sub>1</sub>).

---

<sup>1</sup> Ar. Abanov, A. V. Chubukov, and A.M. Finkelstein, *Europhys. Lett.* **54**, 488 (2001).

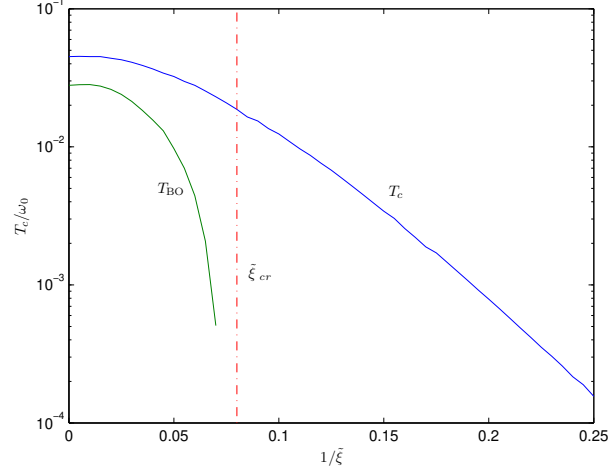


FIG. 18: Superconducting  $T_c$  and the onset temperature  $T_{BO}$  for bond order with diagonal  $\mathbf{Q}$ , as functions of the magnetic correlation length. We set  $\tilde{\kappa} = 0.14$  and  $\tilde{g} = 0.1$ . The red dashed line is  $\tilde{\xi}_{cr}$ , given by Eq. (92).

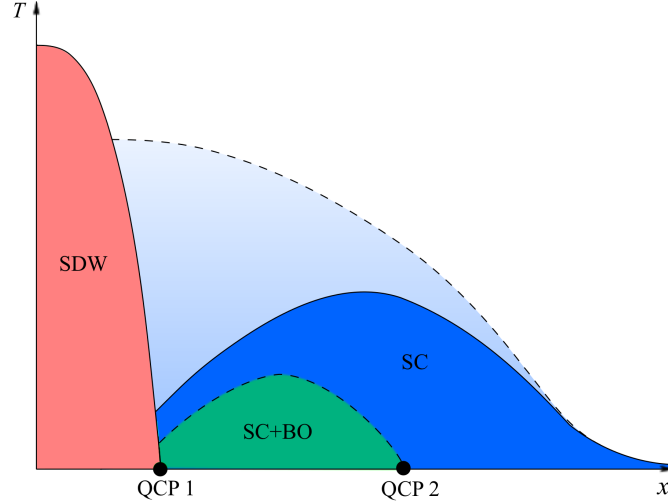


FIG. 19: A schematic phase diagram for the (artificial) case when the only two competing states are superconductivity and bond order with a diagonal  $\mathbf{Q}$ . The light blue region is where the pseudogap phase, which combines superconducting fluctuations at large  $x$  and fluctuations between SC and bond order at small  $x$ .

<sup>2</sup> Ar. Abanov, A. V. Chubukov, and J. Schmalian, *Adv. Phys.* **52**, 119 (2003).

<sup>3</sup> M. A. Metlitski and S. Sachdev, *Phys. Rev. B* **82**, 075128 (2010).

<sup>4</sup> Y. Wang and A.V. Chubukov, *Phys. Rev. Lett* **110**, 127001 (2013).

<sup>5</sup> E-G. Moon and A.V. Chubukov, *J. of Low Temp. Phys.* **161**, p 263 (2010).

<sup>6</sup> R. M. Fernandes, S. Maiti, P. Wolfe, and A. V. Chubukov, *Phys. Rev. Lett.* **111**, 057001 (2013).

<sup>7</sup> G.-W. Chern, R. M. Fernandes, R. Nandkishore, and A. V. Chubukov *Phys. Rev. B* **86**, 115443 (2012).

<sup>8</sup> A.V. Chubukov and O. A. Starykh, *Phys. Rev. Lett.* **110**, 217210 (2013).

<sup>9</sup> S. Sachdev, *Quantum Phase Transitions*, Second Edition, Cambridge University Press (2011).

<sup>10</sup> M. Marciani, L. Fanfarillo, C. Castellani, and L. Benfatto, arXiv:1306.5545.

<sup>11</sup> S. Sachdev and R. La Placa, *Phys. Rev. Lett.* **111**, 027202 (2013).

<sup>12</sup> I. M. Vishik, W. S. Lee, R-H He, M. Hashimoto, Z Hussain, T. P. Devereaux and Z-X Shen, *New J. Phys.* **12** 105008 (2010). Rui-Hua He, *et al.*, *Science* **331**, 1579 (2011).

<sup>13</sup> A. A. Kordyuk, V. B. Zabolotnyy, D. V. Evtushinsky, D. S. Inosov, T. K. Kim, B. Buechner, and S. V. Borisenko, *Eur.Phys.J.* **188**, 153 (2010).

<sup>14</sup> Takeshi Kondo, Ari Palczewski, Yoichiro Hamaya, K. Ogawa, Tsunehiro Takeuchi, J. S. Wen, G. Z. J. Xu, Genda Gu, and Adam Kaminski, arXiv:1208.3448.

- <sup>15</sup> U. Chatterjee, J. Zhao, D. Ai, S. Rosenkranz, A. Kaminski, H. Raffy, Z. Z. Li, K. Kadowaki, M. Randeria, M. R. Norman, and J. C. Campuzano Proc. Nat. Acad. Sci. **108** 9346 (2011).
- <sup>16</sup> H.-B. Yang, J. D. Rameau, Z.-H. Pan, G.D. Gu, P. D. Johnson, H. Claus, D. G. Hinks, and T. E. Kidd Phys. Rev. Lett. **107**, 047003 (2011).
- <sup>17</sup> K. B. Efetov, H. Meier, and C. Pépin, Nat. Phys. (2013)
- <sup>18</sup> D. F. Mross, J. McGreevy, H. Liu, and T. Senthil, Phys. Rev. B **82**, 045121 (2010).
- <sup>19</sup> Ar. Abanov, A. V. Chubukov, and M. R. Norman, Phys. Rev. B **78**, 220507(R) (2008).
- <sup>20</sup> A. V. Chubukov and D. L. Maslov Phys. Rev. B **86**, 155136 (2012); Phys. Rev. B **86**, 155137 (2012).
- <sup>21</sup> W. L. McMillan, Phys. Rev. **167**, 331 (1968).
-